Microglial STAT1-sufficiency is required for resistance to toxoplasmic encephalitis

Cowan, M.N.[1], Kovacs, M.A. [1], Sethi, I. [1], Babcock, I.W. [1], Still, K. [1], Batista, S.J. [1], O'Brien, C.A.[1], Thompson, J.A[1]., Sibley, L.A.[1], Labuzan, S. A.[1], and Harris, T.H.[1]

[1]*Center for Brain Immunology and Glia, Department of Neuroscience, University of Virginia, Charlottesville, VA, United States*

Corresponding Author:

Tajie H. Harris

Email address: tajieharris@virginia.edu

Abstract

Toxoplasma gondii is a ubiquitous intracellular protozoan parasite that establishes a life-long chronic infection largely restricted to the central nervous system (CNS). Constant immune pressure, notably IFN-γ-STAT1 signaling, is required for preventing fatal pathology during *T. gondii* infection. Here, we report that abrogation of STAT1 signaling in microglia, the resident immune cells of the CNS, is sufficient to induce a loss of parasite control in the CNS and susceptibility to toxoplasmic encephalitis during the early stages of chronic infection. Using a microglia-specific genetic labeling and targeting system that discriminates microglia from blood-derived myeloid cells that infiltrate the brain during infection, we find that, contrary to previous *in vitro* reports, microglia do not express inducible nitric-oxide synthase (iNOS) during *T. gondii* infection *in vivo*. Instead, transcriptomic analyses of microglia reveal that STAT1 regulates both (i) a transcriptional shift from homeostatic to “disease-associated microglia” (DAM) phenotype conserved across several neuroinflammatory models, including *T. gondii* infection, and (ii) the expression of anti-parasitic cytosolic molecules that are required for eliminating *T. gondii* in a cell-intrinsic manner. Further, genetic deletion of *Stat1* from microglia during *T. gondii* challenge leads to fatal pathology despite largely equivalent or enhanced immune effector functions displayed by brain-infiltrating immune populations. Finally, we show that microglial STAT1-deficiency results in the overrepresentation of the highly replicative, lytic tachyzoite form of *T. gondii*, relative to its quiescent, semi-dormant bradyzoite form typical of chronic CNS infection. Our data suggest an overall protective role of CNS-resident microglia against *T. gondii* infection, illuminating (i) general mechanisms of CNS-specific immunity to infection (ii) and a clear role for IFN-STAT1 signaling in regulating a microglial activation phenotype observed across diverse neuroinflammatory disease states.

Introduction

Toxoplasma gondii is a ubiquitous protozoan parasite that traffics to the brain, where it establishes a chronic, life-long infection in both humans and mice. Infection with *T. gondii* occurs in two phases: (i) an acute infection wherein parasite disseminates widely throughout host tissues and (ii) a subsequent chronic infection largely restricted to the immune-privileged CNS [reviewed in ref. 1]. Protective immunity during both the acute and chronic phases of *T. gondii* infection converge on cellular responses to the pro-inflammatory cytokine, interferon (IFN)-γ, and its downstream signaling through the transcription factor signal transducer and activator of transcription 1 (STAT1) [2,3]. *Stat1*$^{-/-}$ mice phenocopy *Ifng*$^{-/-}$ mice, succumbing to *T. gondii* infection during the acute stage of infection [4]. Similarly, antibody blockade of IFN-γ during chronic *T. gondii* infection leads to animal mortality, illustrating that interferon signaling is critical for immune resistance during both stages of infection [5].

During both health and disease, microglia, the tissue-resident macrophages of the central nervous system (CNS), play diverse roles in maintaining tissue homeostasis and potentiating inflammation [reviewed in ref. 6]. A large pool of research has focused on studying microglia during neurodevelopmental and neurodegenerative models, yet their functional roles during CNS infection *in vivo* have been less explored. Part of this gap in understanding stems from recent findings that yolk sac-derived microglia are ontogenically, transcriptionally, and functionally distinct from the bone-marrow derived macrophage population that infiltrates the immune-privileged brain during neuroinflammatory states, including CNS infection [7–11]. Microglia have further been shown to rapidly de-differentiate and adopt an inflammatory signature when removed from the brain's unique tissue microenvironment, making *in vitro* approaches inadequate for recapitulating microglial physiology *in vivo* [12,13].

Several studies utilizing pharmacological depletion of microglia by targeting CSF1R during viral CNS infections have collectively revealed that microglia provide protection in controlling viral burden and against host mortality [14–19]. However, CSF1R antagonism alone also depletes macrophages systemically, with multiple studies also pointing to impaired maturation and function of myeloid populations in circulation and lymphoid organs [17,20,21]. CSF1R antagonism has also been reported to elevate baseline levels of pro-inflammatory cytokines in the brains of treated mice [22]. These local and systemic effects thus serve as confounding variables for cell type-specific functional interpretations.

Recently, our group utilized a tamoxifen-inducible cre recombinase system commonly used in neuroinflammatory mouse models to label and assay microglia independently of bone marrow-derived cells [11]. These experiments revealed that microglial but not peripheral macrophage-derived IL-1α is required for brain parasite burden control. We have extended this experimental paradigm to investigate how the microglial response to IFN-γ impacts neuro-immunity by genetically deleting *Stat1* from this cell type. Given that (i) microglia are the primary hematopoietic cell population present in the steady-state brain, and (ii) IFN-γ-STAT1 signaling is essential for anti-parasitic functions across a wide array of cell types, we hypothesized that microglia serve as the brain's first responders in restricting early CNS infection with *T. gondii* via STAT1-mediated signaling.

Here, we report that despite efficient parasite clearance from peripheral tissues during the acute stage of *T. gondii* infection, mice with microglial-specific *Stat1* deletion succumb to severe toxoplasmic encephalitis following uncontrolled parasite replication within the brain. We also find that, despite this severe pathology observed with microglial genetic targeting, the brain-infiltrating immune compartment displays a robust anti-parasitic activation profile. Our studies thus implicate cell-intrinsic roles for microglia in controlling CNS infection with *T. gondii* and highlight an inability

for the peripheral immune system to compensate for STAT1 deficiency in the microglial compartment.

Results

Microglial activation and recruitment to T. gondii foci within the brain. Previous studies have revealed that myeloid cell recruitment from the blood to the *T. gondii*-infected brain are required for preventing fatal toxoplasmic encephalitis [23]. Because microglia and monocyte-derived macrophages are difficult to discriminate via immunohistochemistry, which offers spatial resolution of the infected brain, we generated CX3CR1$^{CreERT2/+}$ x ROSA26$^{Ai6/Ai6}$ (WT) mice to specifically fluorescently label microglia with ZsGreen and discriminate them from monocyte-derived macrophages in the inflamed brain parenchyma [24] (**Fig. 1A**). We opted to use a genetic *in vivo* approach throughout our studies due to multiple studies characterizing rapid microglial de-differentiation and increased activation when removed from the CNS and analyzed in *vitro* [13,25]. Immunohistochemical analyses illustrated that following intraperitoneal challenge and progression to chronic *T. gondii* infection, microglia attain a classic “amoeboid” morphology throughout the brain, typical of activation during neuroinflammatory states (**Fig. 1B-C**). We further observed disrupted microglial spatial tiling and increased microglial recruitment to foci of parasite growth (**Fig. 1D-F**). Our fluorescent labeling approach allowed for detection and discrimination of resident microglia from infiltrating macrophages during CNS infection by both confocal microscopy and flow cytometry, permitting the interrogation of microglial functional roles during *T. gondii* challenge (**Fig. 1B-F, Supplementary Fig. 1A-D**).

In order to identify transcriptional programs activated specifically by microglia during *T. gondii* challenge, we FACS-sorted and performed bulk RNA-sequencing on microglia isolated from naïve and chronically-infected mice using our ZsGreen fluorescent reporter. Differential gene expression analysis revealed an enriched IFN-γ response signature in microglia purified from

infected, relative to naïve mice **(Fig. 1G-H)**. We identified 2,889 upregulated genes and 2,983 downregulated genes in microglia that were significantly differentially expressed during *T. gondii* challenge, relative to uninfected controls. Interestingly, we observed that during infection, microglia displayed a transcriptional activation state suggestive of a disease-associated microglia (DAM) phenotype, which is commonly associated with neurodegeneration and typified by the downregulation of microglial homeostatic genes (including *P2ry12*, *P2ry13*, *Hexb*, *Tmem119*, and *Fcrls*) and concomitant upregulation of microglial disease-associated markers (including *Itgax*, *Apoe*, *Axl*, *Clec7a*) [26,27] (**Fig. 1G**). This phenotype emerged when we compared our list of genes differentially expressed by wild-type microglia isolated from naïve and infected mice against a core list of common genes that are differentially expressed across multiple neurodegenerative conditions, including mouse models for Alzheimer's Disease, multiple sclerosis, amyotrophic lateral sclerosis, and normal aging [28]. As observed in neurodegeneration models [28], we observed that during *T. gondii* challenge, microglia downregulate homeostatic genes (81% of reported genes) and upregulate DAM genes (71% of reported genes). These data illustrate strong concordance between microglial transcriptional state in *T. gondii* infection and the classical DAM phenotype observed in neurodegeneration (**Supplemental Fig. 2A-B**). Given that IFN-γ-STAT1 signaling serves as a dominant pathway driving immune activation and host defense during intracellular parasitic infection [29–32], we focused our efforts on evaluating (i) how microglial *Stat1* deletion impacts host susceptibility to *T. gondii*, (ii) the systems-level effects of this deletion during *T. gondii* challenge, and (iii) a potential role for STAT1 signaling in regulating DAM activation during infection.

***Mice with STAT1-deficient microglia succumb to fatal toxoplasmic encephalitis*.**

Myeloid cells are particularly potent responders to IFN-γ through the production of reactive nitrogen species [33,34] and are capable of serving as antigen-presenting cells during infections [35]. To determine if microglial function during *T. gondii* infection is a similarly essential immune

146 program for defense, we used a *Cx3cr1*-driven tamoxifen (TAM)-inducible system to genetically
147 delete STAT1 from brain-resident microglia, generating $MG^{STAT1\Delta}$ mice (**Fig. 2A**).
148
149 Excision of STAT1 from microglia in $MG^{STAT1\Delta}$ mice was assessed using multiple approaches,
150 including: (i) ZsGreen reporter expression, (ii) direct quantification of *Stat1* relative mRNA
151 expression, and (iii) quantification of STAT1 functional readouts. On average, 99.5% of
152 $CD45^{int}$CD11b+ microglia expressed ZsGreen across TAM-treated animals harboring the
153 microglia reporter construct (**Supplemental Fig. 3A-C**). We also observed a 70-85% knockdown
154 in *Stat1* mRNA expression in microglia isolated from naïve tamoxifen-treated (+TAM) compared
155 to corn oil vehicle-treated (No TAM) littermate controls by RT-qPCR (**Supplementary Fig. 3D**).
156 Because STAT1 is a key transcriptional regulator of major histocompatibility proteins [36–38],
157 MHC II expression served as a functional readout of microglial STAT1 excision. We observed that
158 while 98% of WT microglia expressed MHC II at 12 days post-infection (DPI), 18% of microglia
159 from $MG^{STAT1\Delta}$ mice were MHC II+ at this time point, allowing us to use MHC II expression in
160 microglia as a reliable readout for STAT1 excision across experiments (**Fig. 2B, Supplemental**
161 **Fig. 1E-F**). In line with previous literature [24,39], these data collectively illustrate that the *Cx3cr1*-
162 driven tamoxifen-inducible system is efficient in targeting brain-resident myeloid cells during CNS
163 infection.
164
165 In comparison to WT reporter controls, which display robust resistance to *T. gondii*, we found that
166 $MG^{STAT1\Delta}$ mice succumb to *T. gondii* infection, starting at 17 DPI (**Fig. 2C)**. $MG^{STAT1\Delta}$ mice also
167 display increased brain parasite burden at 12 and 15 DPI, despite equal brain parasite burden
168 when parasite invades the brain around 8 DPI (**Fig 2D-F)**. Quantitative PCR of *T. gondii* genomic
169 DNA indicated that our observed increase in parasite burden was largely restricted to the brain,
170 as parasite burden in lung, liver, and heart tissue revealed no difference in parasite burden at 8
171 DPI, around the peak of the acute peripheral infection (**Supplementary Fig. 4A-C**). Furthermore,

lung, liver, and heart parasite burden decreased substantially from 8 to 15 DPI, indicating robust peripheral clearance of parasite despite increased parasite burden in the CNS (**Supplementary Fig. 4D-F**). Histological examination of hematoxylin and eosin-stained brain slices prepared from mice at 15 DPI additionally revealed widespread liquefactive necrosis in $MG^{STAT1\Delta}$ mice treated with tamoxifen (but not vehicle-treated littermate controls), a hallmark of parasite replication-induced tissue destruction (**Fig. 2G-H)**.

Given the severe pathology seen in *T. gondii*-infected $MG^{STAT1\Delta}$ mice relative to controls, we analyzed several additional parameters to examine the specificity of our experimental model. We analyzed ZsGreen expression in circulating immune cells in both WT and $MG^{STAT1\Delta}$ mice by flow cytometry to identify potential off-target STAT1 deletion in brain-infiltrating immune cells. In contrast to >99% ZsGreen labeling efficiency of brain-resident microglia (**Supplemental Fig. 3C**), we observed that ~1% of total circulating immune cells were ZsGreen+ at 12 DPI, and we observed low frequencies of ZsGreen expression across myeloid and T cell populations (**Supplemental Fig. 3E**). No differences were observed in T cell or myeloid cell counts in circulation at this time point (**Supplemental Fig. 5A-E**). As an additional parameter for evaluating the CNS tissue-specificity of our model, we analyzed the peritoneal immune response during the acute phase of infection (8 DPI). We observed no changes in the number of myeloid cells, T cells, or their iNOS and interferon-γ production at this time point, indicating that functionally equivalent protective immune responses are able to effectively form at the peripheral site of inoculation (**Supplementary Fig. 5F-J**). To assess the potential for differences in microglial activation due to genetic deletion of STAT1 prior to *T. gondii* challenge, we performed morphometric Sholl analysis of microglia in naïve WT and $MG^{STAT1\Delta}$ mice [40]. We found no statistically significant differences in microglial morphology, suggesting comparable baseline microglial activation (**Supplementary Fig. 6A-C**). These findings collectively highlight that STAT1-deletion from a single cell type, brain-

resident microglia, results in a CNS-specific loss of parasite restriction following infection with *T. gondii*.

Brain-infiltrating myeloid cells, but not brain-resident microglia, express iNOS during *T. gondii* challenge.

Nitric oxide is a potent reactive nitrogen molecular species thought to restrict parasite replication by depleting host cell arginine [41] and targeting parasite proteases [42]. Expression of inducible nitric oxide synthase (iNOS) is the primary mechanism by which cells are capable of producing nitric oxide, and the expression of this synthase is regulated by IFN-γ-STAT1 signaling [43]. Previous studies have implicated microglia in restricting *T. gondii* replication via nitric oxide production [23,44]. Further, iNOS-deficient mice display pathology during chronic CNS but not acute peripheral infection, typified by a loss of parasite restriction and necrotizing lesions throughout the brain – suggesting that microglial-derived nitric oxide serves as a specialized anti-toxoplasmic resistance mechanism specific to brain tissue [45]. However, flow cytometric quantification of iNOS+ cells with the use of our microglia-specific fluorescent reporter indicated that brain-resident microglia fail to express iNOS *in vivo*, regardless of STAT1-sufficiency (**Fig. 3A, E, I**). Instead, we found that > 95% of iNOS expression in the brain is accounted for by the brain-infiltrating myeloid compartment, based on $CD45^{hi}$ $CD11b^{+}$ $Ly6C^{+}$ expression (**Fig. 3C, Supplementary Fig. 1G-I)**. These findings underscore that microglia are not producers of this STAT1-driven mechanism despite a shared tissue micro-environment that triggers potent iNOS expression in other myeloid cells. In addition to the absence of microglial iNOS expression, we quantified and detected no significant changes in microglial number from the brains of WT and $MG^{STAT1\Delta}$ mice at 12 or 15 DPI across several experiments (**Fig. 3D, H**).

Microglial STAT1 deletion does not impair the global CNS immune response to T. gondii.

To examine the potential for microglial STAT1 deletion to impair the development of anti-parasitic effector mechanisms in the brain-infiltrating immune compartment of $MG^{STAT1\Delta}$ mice, we immunophenotyped both infiltrating-myeloid and T cell populations. Previous studies have indicated that both monocyte-derived cells and T cells must traffic into the CNS to prevent fatal toxoplasmic encephalitis [5,23]. This concept is clearly illustrated by studies revealing that antibody blockade of CD4+ and CD8+ T cells or monocytic CCR2 results in an inability for these protective immune populations to enter the brain and a subsequent loss of parasite control and animal mortality during chronic CNS infection with *T. gondii* [5,23].

Brain-infiltrating myeloid cells.

At 12 DPI, we observed no difference in the number of brain-infiltrating myeloid cells based on $CD45^{hi}$ $CD11b^{+}$ $Ly6C^{+}$ expression, indicating that circulating myeloid cells are able to effectively traffic to the *T. gondii*-infected brain despite microglial STAT1-deletion (**Fig. 3F**). We further found a statistically significant increase in the iNOS expression of these myeloid cells, suggestive of increased, rather than decreased, activation and effector functions of the infiltrating myeloid compartment in $MG^{STAT1\Delta}$ mice relative to WT controls (**Fig. 3G**). At 15 DPI, there was a clear increase in brain-infiltrating myeloid cell recruitment to the brain, with a further potentiation in their ability to express the anti-parasitic effector protein, iNOS (**Fig. 3J-K**).

Brain-infiltrating CD4+ and CD8+ T cell activation.

In contrast to most peripheral macrophage populations, only a small subset (< 3%) of brain-resident microglia express the professional antigen presentation molecule, MHC II, at baseline [46]. Because STAT1 is a primary transcriptional regulator of MHC II expression [36–38], we investigated MHC II expression on microglia, along with the expression of additional antigen presentation-related molecules (MHC I, CD80, and CD86) that are required for antigen-specific T cell activation [36,37]. In naïve mice, we find that few microglia express any of these antigen

presentation molecules (**Supplementary Fig. 7A**). During *T. gondii* infection, however, the expression of MHC I, MHC II, and CD86 was upregulated by microglia in a STAT1-dependent manner (**Supplementary Fig. 7A-D**). Despite the STAT1-dependency of these antigen presentation molecules, we quantified no impairment in T cell activation at multiple time-points during infection in $MG^{STAT1\Delta}$ mice. At 12 DPI, $MG^{STAT1\Delta}$ mice displayed no statistically significant changes in $CD3^+CD4^+$ or $CD3^+CD8^+$ T cell numbers within the brain, and they showed a two-fold increased frequency of IFN-γ+ expression of both T cell sub-types by flow cytometry, relative to WT controls (**Fig. 4A-D, Supplementary Fig. 1J-M**). By 15 DPI, $MG^{STAT1\Delta}$ mice had a three- and two-fold increase in $CD3^+CD4^+$ and $CD3^+CD8^+$ T cell numbers in the brain, respectively, with an increased frequency of CD4+ T cell IFN-γ production (**Fig. 4E-H**). Collectively, analyses of the T cell presence and functional responses in $MG^{STAT1\Delta}$ mice indicate increased, rather than decreased, T cell activation. Further, these results do not suggest that a loss of microglial antigen presentation machinery underpinned the inability to restrict parasite burden in $MG^{STAT1\Delta}$ brains.

Whole brain RNA analysis.

We performed RT-qPCR analysis of mRNA isolated from homogenized brain tissue to examine the expression of a larger panel of immune mediators of resistance against *T. gondii*. In addition to increased *Nos2* (iNOS) gene expression at the tissue-level, $MG^{STAT1\Delta}$ mice showed an overall equivalent (12 DPI) or increased (15 DPI) expression of several chemokines (*Ccl2, Ccl5, Cxcl9, Cxcl10*), pro-inflammatory cytokines (*Ifng*, *Il6*, *Tnfa*), and adhesion molecules (*Icam1*, *Vcam1*) identified in previous literature as conferring resistance against *T. gondii* infection [5,11,47–52] (**Supplementary Fig. 8A-B**). Together, these data indicate that a robust set of anti-parasitic immune mediators are present at the tissue-level, and suggest that neither the brain-infiltrating immune compartment nor other brain-resident cell types are able to compensate for a STAT1 signaling defect within the brain's microglial compartment. We thus focused further efforts on identifying microglial-intrinsic mechanisms of *T. gondii* restriction.

STAT1-deficient microglia display transcriptionally impaired cell-intrinsic immune activation and effector capacity.

In order to attain an unbiased transcriptional overview of how STAT1 regulates microglial immune effector capacity, we FACS-sorted and performed RNA-sequencing on brain-resident microglia from *T. gondii*-infected WT and MG$^{STAT1\Delta}$ mice. (**Fig. 5A-F**). Gene ontology (GO) analysis for biological pathways suggested that relative to WT microglia, STAT1-deficient microglia failed to display the transcriptional signatures of immune defense responses, with GO terms including "response to interferon" and "defense response to protozoan" (**Fig. 5A**). Paired differential gene expression analysis indicated that 1,261 genes were significantly enriched in WT microglia, and 831 genes were significantly enriched in STAT1-null microglia (**Fig. 5B**). Two key themes emerged from our differential gene expression analysis of microglia isolated from *T. gondii*-infected brains: (i) STAT1-null microglia display an impaired ability to acquire a disease-associated microglia (DAM) phenotype observed across several neuroinflammatory disease states [26,27], and (ii) these cells further fail to express key cytosolic genes required for killing intracellular parasite in a cell-intrinsic manner.

STAT1-deficient microglia fail to acquire a cell activation phenotype conserved across diverse neuroinflammatory states.

Given our observations that microglia in the *T. gondii*-infected brain display strong transcriptional overlap with DAMs observed during neurodegeneration, we sought to determine whether STAT1 signaling regulated the DAM phenotype (**Fig. 1G, Supplementary Fig. 2**). Similarly to our transcriptomic analysis of WT naïve vs. infected microglia, we compared our WT vs MG$^{STAT1\Delta}$ differential gene expression dataset to a dataset of DAM genes shared across several neurodegenerative disease states [26]. Because the DAM phenotype is characterized by both the downregulation of microglial homeostatic genes and the upregulation of unique disease-

associated markers during neuroinflammation, we explored both features of the transcriptional signature. We observed during *T. gondii* challenge that relative to wildtype microglia, STAT1-deficient microglia: (i) failed to downregulate 23.5% of all microglial "homeostatic genes" (including *Cx3cr1*, *Tgfb1*, and *Fcrls*) and (ii) failed to upregulate 32% of all DAM-specific genes (including *Itgax*, *Axl*, *Gpnmb*, and *Cybb*) reported in *Krasemann et al. 2017* (**Figure 5C-D**). In addition to highlighting that STAT1-deficient microglia retain a more homeostatic and less inflammatory transcriptional signature relative to controls during *T. gondii* infection, these data point to STAT1 signaling as an integral component of a shared microglial transcriptional profile that is conserved across varying models of neuroinflammation.

STAT1-deficient microglia fail to upregulate genes encoding critical anti-parasitic cytosolic proteins.

To determine specific STAT1-dependent mechanisms that could explain a functional loss of parasite restriction in $MG^{STAT1\Delta}$ mice, we performed further differential gene expression analysis. We analyzed each of the genes within the Gene Ontology term, "Defense response to protozoan" (GO:0042832) and found that 44% of annotated genes were expressed at significantly lower levels in STAT1-null microglia (**Fig. 5E**). Amongst the most highly differentially expressed genes between WT and $MG^{STAT1\Delta}$ microglia, we observed robust STAT1-dependent expression of several cytosolic anti-parasitic killing genes (**Fig. 5E-F**). These genes included immunity-related GTPases (IRGs) and guanylate-binding proteins (GBPs), both families of which have been implicated in cooperatively contributing to the mechanical killing and intracellular clearance of *T. gondii* from both hematopoietic and non-hematopoietic cell types [53–57]. We identified several additional IRGs (*Igtp*, *Irgm1*, *Tgtp1*, *Ifi47*) and *Gbp10* that were expressed in microglia in a STAT1-dependent manner (**Fig 5F**). These data identifying the lack of large families of cell-intrinsic parasite killing genes, in tandem with a lack of observable effects of microglial STAT1 deletion on the global, cell-extrinsic immune response, support the hypothesis that cell-intrinsic parasite killing

may serve as a primary mechanism of STAT1-dependent microglial parasite restriction. In the absence of this cytosolic restriction, we hypothesized that microglial STAT1-deficiency would generate a replicative niche in which *T. gondii* can expand.

Microglial STAT1-deficiency results in a skewing of T. gondii toward its replicative form. Consistent with the hypothesis that microglial STAT1 deletion provides a replicative niche for the parasite, we observed increased microglial co-localization with large foci of reactive *T. gondii* lesions in the brains of $MG^{STAT1\Delta}$ mice, which has been previously described as characteristic of the highly-replicative and lytic tachyzoite form of *T. gondii,* rather than its semi-dormant bradyzoite (cystic) form [58] (**Fig 6A-B**). We then analyzed the prevalence and ratio of these two infectious forms of the parasite in $MG^{STAT1\Delta}$ and WT mice via RT-qPCR. Three primers were designed for *T. gondii*-specific genes: (i) *Sag1*, a gene expressed selectively in tachyzoites (replicative form); (ii) *Bag1*, expressed by slowly replicating bradyzoites (quiescent form); and (iii) *Act1*, expressed by both forms of *T. gondii* [59–61]. While WT brains displayed a one-fold increase in *Bag1* to *Act1* ratio relative to $MG^{STAT1\Delta}$ brains, we observed a nearly 150-fold increase in the tachyzoite gene *Sag1* normalized to *Act1* at 15 DPI in $MG^{STAT1\Delta}$ relative to WT brains, and thus a 300-fold increase in the ratio of *Sag1* relative to *Bag1* with STAT1-deficiency (**Fig. 6C-E**). These data confirm that relative to WT controls, $MG^{STAT1\Delta}$ brains are highly skewed toward a replicative and lytic form of *T. gondii*. Further consistent with microglial STAT1-deletion permitting a parasite replicative niche, we were able to identify microglia filled with tachyzoite rosettes via confocal microscopy in the brains of $MG^{STAT1\Delta}$ but not WT mice (**Fig. 6F-G**).

Discussion

Here, we find that abrogation of STAT1 signaling in brain-resident microglia results in a severe susceptibility to CNS infection with *T. gondii*, despite robust immune effector functions in the brain-infiltrating immune compartment and efficient parasite clearance in peripheral tissues –

352 highlighting a requirement for microglial-intrinsic parasite control. Importantly, we show that
353 contrary to interpretations from previous literature [44], microglia do not express iNOS during *in*
354 *vivo T. gondii* challenge. Instead, transcriptomic analysis suggests that a loss of STAT1-regulated
355 cytosolic killing genes, including those from the IRG and GBP superfamilies, may normally play a
356 role in preventing microglia from serving as a cellular niche in which *T. gondii* can freely replicate.
357 Consistent with this model, we observe that STAT1-deficiency in microglia results in an increased
358 brain parasite burden and a skewing of parasite towards its fast-replicating and lytic tachyzoite
359 form within the brain.
360
361 As with any study, there are caveats and limitations that must be appropriately considered in
362 interpreting the presented data. Importantly, the CX3CR1^{CreERT2} system allows for substantial
363 turnover of short-lived circulating immune cells [24,62] but is expected to additionally target other
364 tissue-resident macrophage populations [62,63]. Experiments were performed to verify effective
365 parasite clearance and immunity in peripheral tissues, but there exists a relatively small but long-
366 lived CX3CR1+ population of border-associated CNS macrophages (BAMs), located along CNS
367 interfaces [63]. We expect that tamoxifen treatment may yield STAT1-deficient BAMs, such as
368 perivascular and choroid plexus macrophages, which may be spatially positioned to encounter *T.*
369 *gondii* before it breaches into the brain parenchyma. While we did not observe increased parasite
370 burden at 8 DPI, when parasite is seeding the brain between MG$^{STAT1\Delta}$ and WT mice, future
371 experiments are necessary to determine whether BAMs play an active role in parasite restriction,
372 and whether these roles are similar to those of microglia.
373
374 Our finding that STAT1-deficiency in microglia leads to a 300-fold increase, relative to WT
375 controls, in the replicative tachyzoite form of *T. gondii*, is well-framed within the context of a
376 previous study that examined the role of STAT1 signaling in astrocytes [64]. We observe multiple
377 similarities between our data and this study: (i) increased animal mortality, (ii) increased brain

parasite burden, (iii) liquefactive necrosis throughout the brain, and (iv) a loss of IRG and GBP expression with concomitant susceptibility of the targeted STAT1-deficient cell type to *T. gondii* parasitization. Our study dovetails with this previous publication in illustrating the essential role of STAT1 signaling in both hematopoietic and non-hematopoietic cell types, and suggests that many different cell types may be able to serve as replicative niches for this opportunistic pathogen in the absence of STAT1. However, there are important differences observed between microglial and astrocytic STAT1 deletion during *T. gondii* infection that may be informative in better understanding cell type-parasite interactions.

First, the animal mortality observed in $MG^{STAT1\Delta}$ mice in our study occurs more rapidly (~17 DPI) than as reported with astrocytic STAT1-deletion (~25 DPI), and with greater penetrance, indicating more severe disease pathology [64]. Second, $MG^{STAT1\Delta}$ mice display potentiated, rather than equivalent, T cell and infiltrating myeloid functional responses [64]. Third, astrocytic STAT1-deletion appears to promote the bradyzoite form of *T. gondii*, whereas $MG^{STAT1\Delta}$ mice show strong bias toward the tachyzoite form of *T. gondii* [64]. Different physiological properties of these two glial populations may offer insights into these key differences in phenotype. Microglia, relative to astrocytes, are highly motile cells with a complex sensome that drives chemotactic responses to tissue damage or disruption [65–68], as is evident in our confocal images of microglia abandoning their evenly-tiled territories and clustering around *T. gondii* tachyzoites at multiple time-points, regardless of STAT1-sufficiency. Rapid migration of STAT1-sufficient microglia to sites of lytic tachyzoite egress may thus position these cells to serve as an immunological “cellular buffer” – becoming actively infected and subsequently clearing intracellular infection via STAT1-dependent cytosolic killing molecules. In the absence of STAT1 signaling, this chemotactic response may contrastingly permit the parasite to be more rapidly passaged through a hospitable cell type that is unable to mount a cell-intrinsic immune response, thus potentially overwhelming brain tissue. Future studies will be needed to understand if the observed skewing of parasite form toward its

tachyzoite state reflects an inability for tachyzoites to convert to bradyzoites due to intrinsic properties of microglia, or alternatively reflect an interaction of STAT1 signaling abrogation with unknown biological factors of early-chronic infection (15 DPI).

Our data also provide multiple insights to a broader understanding of microglial identity and their physiology across disease states. While most macrophages typically display remarkable plasticity attuned to their tissue microenvironments [8,69,70], the observation that microglia do not express iNOS, despite sharing an interferon-primed environment with iNOS+ infiltrating myeloid cells, indicates that these two cell populations provide differential immune effector functions during *T. gondii* infection. This differential expression of immune effector mechanisms mirrors previous work from our lab showing that microglia, unlike infiltrating macrophages: (i) express low levels of IL-1β during chronic infection, and (ii) display a comparatively dampened NF-κB signature during *T. gondii* challenge [11]. In the present study, we also find that microglia acquire a neurodegenerative-like DAM signature during *T. gondii* infection, and that this signature is partially regulated by STAT1 signaling during parasitic infection. While caution must be exercised in attributing the DAM phenotype to parasite restriction, this gene expression signature highlights an inability of STAT1-deficient microglia to acquire the cell type-specific transcriptional hallmarks of immune activation conserved across other neuroinflammatory models. Future studies targeting genes such as TREM2 or APOE, which have been shown to regulate the microglial transition to DAMs, may be needed to discern whether DAMs are, in themselves, neuroprotective during CNS infection. Similarly, future experiments using $MG^{STAT1\Delta}$ mice in models of neurodegeneration may additionally yield novel insights into how the microglial response to interferon shapes or mitigates disease progression in a wide range of disease models.

Materials and Methods

Mice. CX3CR1^{CreERT2} (#020940) and ROSA26$^{Ai6/Ai6}$ (#007906) mouse lines were originally purchased from Jackson Laboratories and cross-bred to generate CX3CR1^{CreERT2} x ZsGreen$^{fl/stop/fl}$ mice used as controls. These control mice were subsequently cross-bred with STAT1$^{fl/fl}$ mice (provided by Lothar Hennighausen, NIH) to generate STAT1$^{fl/fl}$ x CX3CR1^{CreERT2} x ROSA26$^{Ai6/Ai6}$ (MG$^{STAT1\Delta}$) mice. Age- and sex-matched mice were intraperitoneally administered tamoxifen (4 mg per 20 g body weight, Sigma-Aldrich) between 4-7 weeks of age for 5 consecutive days to induce STAT1 deletion. Four weeks following tamoxifen treatment, mice were challenged with the type II *T. gondii* strain Me49 or proceeded with naïve experiments. Parasite was passaged through CBA/J and Swiss Webster mice (Jackson Laboratories), and mice used in infection experiments were intraperitoneally challenged with 10 Me49 cysts from CBA/J brain homogenate. *Stat1* excision was confirmed by qPCR, flow cytometry, or immunohistochemistry. All mice were housed in University of Virginia specific pathogen-free facilities with a 12h light/dark cycle, with ambient temperature between 68 and 72 F, and 30-60% humidity. Mice used in experiments were euthanized by CO_2 asphyxiation if they showed weight loss greater than 20% of their baseline, pre-recorded weight. All procedures were approved and conducted in accordance with the University of Virginia Institutional Animal Care and Use Committee approval of protocol 3968.

Immunohistochemistry. PBS-perfused brain hemispheres were fixed in 4% paraformaldehyde (Electron Microscopy Sciences) for 24 hours at 4°C. Brains were then cryopreserved in a 30% sucrose solution for 48 hours at 4°C, flash-frozen in OCT (Sakura), on dry ice, and cryosectioned at a thickness of 50 µm. Free-floating sections were blocked for 1 hour at room temperature in a 1x PBS solution containing 0.1% Triton, 0.05% Tween 20, 5% BSA, and 0.1% BSA. Sections were incubated in primary antibodies overnight at 4°C. Sections were washed with a 1x PBS, 0.05% Tween solution prior to incubation in primary antibodies for one hour at RT. Following secondary washes, sections were incubated in DAPI (Thermo Fisher Scientific) for 5 minutes and mounted on glass coverslips (Thermo Fisher Scientific) in Aquamount (Lerner Laboratories)

455 mounting media. Dilutions were performed at a 1:200 concentration for primary antibodies and a
456 1:1,000 concentration for secondary antibodies and DAPI staining. All immunohistochemical
457 micrographs were captured using a Leica TCS SP8 Confocal microscope. Images were analyzed
458 using Imaris or ImageJ software. Primary antibodies used in experiments included goat anti-Iba1
459 (Abcam), rabbit anti-Me49 (gift from Fausto Araujo), and rat anti-MHC II (Cat. #: 14-5321-82;
460 Thermo Fisher Scientific). Secondary antibodies used in experiments included: Alexa Fluor 594
461 Donkey Anti Rabbit IgG (Cat. #: 711-585-152; Jackson ImmunoResearch), Alexa Fluor 647
462 Donkey Anti-Rabbit IgG (Cat. #: 711-605-152; Jackson ImmunoResearch), Cy3 AffiniPure
463 Donkey Anti Rat IgG (Cat. #: 712-165-153; Jackson ImmunoResearch).
464
465 **Sholl Analysis**. Sholl analysis was used to analyze microglial morphological complexity as a
466 readout for their activation state, in accordance with the protocol published in *Norris et al., 2014*
467 [40]. In brief, confocal photomicrographs of naive WT and $MG^{STAT1\Delta}$ brains with ZsGreen+
468 microglia were captured and analyzed in Fiji with the Sholl Analysis plugin software. Images were
469 processed in binary pixels, microglia were manually selected, and shells were inserted in 5 µm
470 concentric circles, starting from 10 µm outside the center of the soma, and ending at the limit of
471 the longest arborization for each analyzed microglia. The number of dendritic intersection points
472 was plotted for each distance away from the soma, and data was analyzed via 2-way ANOVA
473 with Sidak's multiple comparison test.
474
475 ***H&E Tissue staining.*** Brains were fixed in formalin, prior to being embedded in formalin,
476 sectioned, and stained with hematoxylin and eosin at the UVA Research Histology Core.
477 Following mounting, sections were imaged on a DM 2000 LED brightfield microscope (Leica
478 Biosystems).
479

480 ***Tissue Processing.*** Mice were given an overdose of ketamine/xylazine and transcardially
481 perfused with 30 mL of ice-cold 1X PBS. Brains and spleen were collected and placed in cold
482 complete RPMI media (cRPMI) (10% FBS, 1% sodium pyruvate, 1% non-essential amino acids,
483 1% penicillin/streptomycin, and 0.1% 2-ME). Brains were minced with a razor blade, passed
484 through an 18G needle, and enzymatically digested with 0.227 mg/mL collagenase/dispase and
485 50U/mL DNase (Roche) for 45 minutes at 37C. If brain samples were used to quantify parasite
486 burden or for gene expression analysis, aliquots were removed and frozen for downstream
487 analysis prior to addition of digestion enzymes. If brain cells were being used for downstream
488 RNA sequencing for WT vs. $MG^{STAT1\Delta}$ analysis, Actinomycin D (Sigma-Aldrich) was added to the
489 digestion buffer at a concentration of 45 µm during incubation and 3 µm during washes to inhibit
490 upregulation of immediate early activation genes associated with subsequent FACs sorting. All
491 brain samples were resuspended in 20 mL of 40% percoll and spun for 25 minutes at 650 xg to
492 remove myelin. Following myelin removal, samples were washed with and subsequently
493 resuspended in cold cRPMI. Blood collected for flow cytometric analysis was isolated from the
494 heart prior to transcardial perfusion and transferred into 1x PBS + EDTA (Thermo Fisher
495 Scientific). Blood was then processed with RBC lysis and resuspended in cold cRPMI prior to
496 staining and fixation for flow cytometry. For peritoneal lavage experiments, 5 mL of cold 1X PBS
497 was injected through the membrane encasing the peritoneal cavity via a 26G needle and
498 withdrawn with a 22G needle. Lavage fluid was washed and suspended in cRPMI.
499
500 ***Flow cytometry***. Following generation of a single-cell suspension, cells were plated in a 96-well
501 plate and incubated for 10 minutes in 50 µL Fc block (1 µg/mL 2.4G2 Ab (BioXCell), 0.1% rat γ-
502 globulin (Jackson ImmunoResearch) at room temperature. Cells were incubated in primary
503 antibodies at a concentration of 1:200, and AF-780 viability dye (eBioscience) at a concentration
504 of 1:800 for 30 minutes at 4°C. Antibody clones used for experiments included: MHC II
505 (M5/114.15.2), CD11b (M1/70), Ly6C (HK1.4), iNOS (CXNFT), CD45 (30-F11), CD3e (145-

2C11), CD4 (GK1.5), CD8a (53-6.7), and IFN-γ (XMG1.2) (Thermo Fisher Scientific). After staining for surface markers, cells were washed and fixed overnight in 2% PFA at 4°C, before being washed and intracellularly stained, if quantifying cytosolic protein. For intracellular cytokine staining (IFN-γ), initial single cell suspensions were incubated with Brefeldin A (Selleckchem) for 5 hours at 37°C prior to blocking and staining. For intracellular staining, cells were permeabilized with Permeabilization Buffer (eBioscience) and stained for 30 minutes at room temperature. Cells were washed with FACS buffer and transferred into 5 mL FACS tubes, then were analyzed on a Gallios flow cytometer (Beckman-Coulter). Flow cytometry data was analyzed using FlowJo.

Cell Sorting / Enrichment. For RNA sequencing and analysis of microglial *Stat1* relative expression to validate excision, brains were processed into a single cell suspension, as described above. Cells were then magnetically labeled with CD11b-conjugated beads diluted in MACS buffer for 15 minutes, per manufacturer's instructions. Following a wash with 2 mL of MACS buffer, samples were spun at 1500 RPM for 5 minutes and resuspended in 600 uL of MACS buffer. Myeloid cells were then positively selected for using anti-CD11b-conjugated magnetic beads enrichment (Miltenyi). Cells were resuspended and lysed in Trizol for RT-qPCR analysis, or incubated for 10 minutes in 50 µL Fc block (1 µg/mL 2.4G2 Ab (BioXCell), 0.1% rat γ globulin (Jackson ImmunoResearch) at room temperature for RNA-sequencing. Cells were stained with the following antibodies (Thermo Fisher Scientific) for 30 minutes at 4°C: CD11b-Percp Cy5.5 (Cat. #45-0112-82), MHCII-eFluor 450 (Cat. # 48-5321-82), CD45-APC (Cat. #17-0451-81), Ly6C-PE Cy7 (Cat. #12-5932-80), CD3e-PE Cy7 (Cat. #25-0031-81), NK1.1-PE Cy7 (Cat. #25-5941-81), CD19-PE Cy7 (Cat. #25-0193-81). Live cells were analyzed and sorted using a BD Aria flow cytometer at the University of Virginia Flow Cytometry Core facility. Cells were sorted based on ZsGreen and dump gating ($CD3e^-$ $NK1.1^-$ $CD19^-$ $Ly6C^-$) directly into Trizol (Invitrogen) for RNA

extraction and RNA sequencing. For MG$^{STAT1\Delta}$ mice, MHC II^{neg} microglia were gated in order to positively select for STAT1-deficient cells.

Quantitative RT-PCR. For tissue-level analysis, one-fourth of a mouse brain was placed in 1 mL Trizol (Ambion), mechanically homogenized using 1 mm zirconia/silica beads (Biospec) for 30 seconds using a Mini-BeadBeater 16 (BioSpec). For gene expression analysis of magnetically-enriched cells, cells were homogenized in Trizol by pipetting. RNA was extracted from Trizol according to manufacturer's instructions (Invitrogen). High Capacity Reverse Transcription Kit (Applied Biosystems) was used to generate cDNA. Quantitative PCR was performed using 2X Taq-based Master Mix (Bioline) and TaqMan gene expression assays (Applied Biosystems), or custom primers (Integrated DNA Technologies), run on a CFX384 Real-Time System thermocycler (Bio-Rad Laboratories). Murine *Hprt* and *T. gondii Act1* were used for normalization for analyzing host and parasite gene expression, respectively, and relative expression is reported as $2^{(-\Delta\Delta CT)}$. The following Thermo Fisher mouse gene probes were used: *Stat1* (Mm00439518_m1), *Hprt* (Mm00446968_m1), *Ifng* (Mm01168134_m1), *Nos2* (Mm00440502_m1), *Il6* (Mm00446190_m1), *Icam1* (Mm00516023_m1), *Vcam1* (Mm01320970_m1), *Tnfa* (Mm00443258_m1), *Ccl2* (Mm00441242_m1), *Ccl5* (Mm01302427_m1), *Cxcl9* (Mm00434946_m1), *Cxcl10* (Mm00445235_m1). Custom primers for used for analyzing *T. gondii* genomic DNA and gene expression were used and are provided in **Supplementary Table 1**.

RNA sequencing analysis. RNA reads from FASTQ files were trimmed and filtered using Trimmomatic (v0.39) paired-end set to phred 33 quality scoring. Adapters were trimmed, and reads with a minimum quality score of 15, leading and trailing quality scores of 3, and minimum fragment length of 36 were used for analysis. FastQC (v0.11.9) was used to verify quality of sample reads. Trimmed and filtered reads were aligned to thee GENCODE M13 reference

557 genome using Salmon (v0.8.2) and output as .sam files. Transcript abundance files were imported
558 into R (v4.1.1) and converted to gene abundances using Tximport (v1.24.0). The R Bioconductor
559 package, DESeq2 (v1.36.0), was used to perform differential expression analysis. DESeq2-
560 normalized data was visualized using the following R packages: EnhancedVolcano (v1.14.0),
561 pHeatmap (v1.0.12), and ggplot2 (v3.3.6). Gene names were converted from mouse ENSEMBL
562 gene identifiers to gene symbols using the Bioconductor BiomaRT (v2.52.0) database. Labeled
563 genes were manually selected from significantly differentially expressed genes from the DESeq2
564 results data frame. All genes with a Benjamini-Hochberg (BH) adjusted p-value below 0.05 were
565 considered significantly upregulated if they had a log2FC > 0, and downregulated if they had a
566 log2FC < 0. In order to determine Gene Ontology (GO) enrichment analysis for biological
567 processes was performed by running a list of significantly differentially expressed genes and their
568 p-values through TopGO (v2.48.0). Enrichment score is reported as the $-\log_{10}$ of enrichment p
569 value, based on Kolmogorov-Smirnov (KS) analysis. Significantly enriched GO Terms were
570 selected and plotted based on biological interest. For analysis of the DAM signature, the full list
571 of common genes upregulated (disease-associated microglia genes) and downregulated by
572 microglia (homeostatic genes) across disease conditions in *Krasemann et al., 2017* was analyzed
573 in our dataset, and significantly differentially expressed genes from this list were plotted. For
574 targeted analysis of anti-parasitic genes, the full list of unique annotated genes in the GO:0042832
575 Term ("Defense Response to Protozoan") was analyzed within our dataset, and all significantly
576 differentially expressed genes were plotted.
577
578 ***Statistics***. Data from multiple experiments within a given time-point were aggregated to reflect
579 biological variability from different infections. When data from multiple infection cohorts were
580 compiled, a randomized block ANOVA test (two-way) was performed in R. This statistical test was
581 selected to evaluate the effect of treatment group, while controlling for infection date as a variable
582 that was statistically modeled as a random effect contained in our datasets. Data from Kaplan-

583 Meier curves, flow cytometric analyses, and qPCR results were graphed using GraphPad Prism,
584 and data related to transcriptomic analysis were graphed using R. Error bars indicate standard
585 error of the mean (SEM). Statistical tests used for each reported experiment are detailed within
586 figure legends. Normal distributions for each population are assumed for statistical testing.
587
588 **Data availability.** RNA sequencing data have been deposited in GEO under the accession codes:
589 GSE204751, GSE146680, and GSE203655. For graphs that visualize compiled experimental
590 group means (**Fig. 3D-K**, **Fig. 4A-H,** and **Supplementary Fig. 5**), data points for individual mice
591 are available on Dryad: doi:10.5061/dryad.fttdz08w2.
592
593 **Acknowledgements**
594 The authors would like to thank members of the Harris Lab, Center for Brain Immunology and
595 Glia (BIG), Carter Immunology Center (CIC), and Neuroscience Graduate Program at the
596 University of Virginia for their input in the development of this work. We also would like to thank
597 Will Rosenow, Marieke Jones, PhD, and Christopher Overall, PhD for their assistance with the
598 computational analysis of RNA-sequencing data, as well as the UVA Flow Cytometry Core,
599 Research Histology Core, Health Sciences Library, and Research Computing for methodological
600 assistance. We thank Lothar Hennighausen (NIH) for gifting us STAT1$^{fl/fl}$ mice that were used to
601 generate experimental mice, and Fausto Araujo (Palo Alto Medical Foundation) for gifting us the
602 anti-Me49 antibody used in experiments. Parts of Figure 1 and 2 were created with
603 Biorender.com. This work was funded by National Institutes of Health grants R01NS112516 and
604 R56NS106028 to T.H.H., T32AI007496 to M.N.C., T32AI007496, T32GM007267, and
605 F30AI154740 to M.A.K., T32AI007046 to S.J.B., T32GM008328 to K.M.S., T32AI007496 to
606 C.A.O., T32AI007496 to I.W.B., and by the UVA Double Hoo Award to M.N.C. and I.S.
607

References

1. Matta SK, Rinkenberger N, Dunay IR, Sibley LD. Toxoplasma gondii infection and its implications within the central nervous system. Nat Rev Microbiol. 2021;19: 467–480. doi:10.1038/s41579-021-00518-7

2. Suzuki Y, Remington JS. The effect of anti-IFN-gamma antibody on the protective effect of Lyt-2+ immune T cells against toxoplasmosis in mice. J Immunol. 1990;144: 1954 LP – 1956. Available: http://www.jimmunol.org/content/144/5/1954.abstract

3. Gazzinelli RT, Hakim FT, Hieny S, Shearer GM, Sher A. Synergistic role of CD4+ and CD8+ T lymphocytes in IFN-gamma production and protective immunity induced by an attenuated Toxoplasma gondii vaccine. J Immunol. 1991;146: 286 LP – 292. Available: http://www.jimmunol.org/content/146/1/286.abstract

4. Lieberman LA, Banica M, Reiner SL, Hunter CA. STAT1 Plays a Critical Role in the Regulation of Antimicrobial Effector Mechanisms, but Not in the Development of Th1-Type Responses during Toxoplasmosis. J Immunol. 2004;172: 457–463. doi:10.4049/jimmunol.172.1.457

5. Gazzinelli R, Xu Y, Hieny S, Cheever A, Sher A. Simultaneous depletion of CD4+ and CD8+ T lymphocytes is required to reactivate chronic infection with Toxoplasma gondii. J Immunol. 1992;149: 175–180.

6. Prinz M, Jung S, Priller J. Microglia Biology: One Century of Evolving Concepts. Cell. 2019;179: 292–311. doi:10.1016/j.cell.2019.08.053

7. Ginhoux F, Greter M, Leboeuf M, Nandi S, See P, Gokhan S, et al. Fate mapping analysis reveals that adult microglia derive from primitive macrophages. Science (80-). 2010. doi:10.1126/science.1194637

8. Bennett FC, Bennett ML, Yaqoob F, Mulinyawe SB, Grant GA, Hayden Gephart M, et al. A Combination of Ontogeny and CNS Environment Establishes Microglial Identity. Neuron. 2018;98: 1170-1183.e8. doi:10.1016/j.neuron.2018.05.014

9. Shemer A, Grozovski J, Tay TL, Tao J, Volaski A, Süß P, et al. Engrafted parenchymal brain macrophages differ from microglia in transcriptome, chromatin landscape and response to challenge. Nat Commun. 2018;9: 5206. doi:10.1038/s41467-018-07548-5

10. Cronk JC, Filiano AJ, Louveau A, Marin I, Marsh R, Ji E, et al. Peripherally derived macrophages can engraft the brain independent of irradiation and maintain an identity distinct from microglia. J Exp Med. 2018;215: 1627–1647. doi:10.1084/jem.20180247

11. Batista SJ, Still KM, Johanson D, Thompson JA, O'Brien CA, Lukens JR, et al. Gasdermin-D-dependent IL-1α release from microglia promotes protective immunity during chronic Toxoplasma gondii infection. Nat Commun. 2020;11: 3687. doi:10.1038/s41467-020-17491-z

12. Butovsky O, Jedrychowski MP, Moore CS, Cialic R, Lanser AJ, Gabriely G, et al. Identification of a unique TGF-β–dependent molecular and functional signature in microglia. Nat Neurosci. 2013;17: 131–143. doi:10.1038/nn.3599

13. Bohlen CJ, Bennett FC, Tucker AF, Collins HY, Mulinyawe SB, Barres BA. Diverse Requirements for Microglial Survival, Specification, and Function Revealed by Defined-Medium Cultures. Neuron. 2017;94: 759-773.e8. doi:10.1016/j.neuron.2017.04.043

14. Waltl I, Käufer C, Gerhauser I, Chhatbar C, Ghita L, Kalinke U, et al. Microglia have a protective role in viral encephalitis-induced seizure development and hippocampal damage. Brain Behav Immun. 2018;74: 186–204. doi:10.1016/j.bbi.2018.09.006

15. Fekete R, Cserép C, Lénárt N, Tóth K, Orsolits B, Martinecz B, et al. Microglia control the spread of neurotropic virus infection via P2Y12 signalling and recruit monocytes through P2Y12-independent mechanisms. Acta Neuropathol. 2018;136: 461–482. doi:10.1007/s00401-018-1885-0

16. Wheeler DL, Sariol A, Meyerholz DK, Perlman S. Microglia are required for protection against lethal coronavirus encephalitis in mice. J Clin Invest. 2018;128: 931–943. doi:10.1172/JCI97229

17. Funk KE, Klein RS. CSF1R antagonism limits local restimulation of antiviral CD8+ T cells during viral encephalitis. J Neuroinflammation. 2019;16: 22. doi:10.1186/s12974-019-1397-4

18. Goddery EN, Fain CE, Lipovsky CG, Ayasoufi K, Yokanovich LT, Malo CS, et al. Microglia and Perivascular Macrophages Act as Antigen Presenting Cells to Promote CD8 T Cell Infiltration of the Brain. Front Immunol. 2021;12. doi:10.3389/fimmu.2021.726421

19. Mangale V, Syage AR, Ekiz HA, Skinner DD, Cheng Y, Stone CL, et al. Microglia influence host defense, disease, and repair following murine coronavirus infection of the central nervous system. Glia. 2020. doi:10.1002/glia.23844

20. Mok S, Koya RC, Tsui C, Xu J, Robert L, Wu L, et al. Inhibition of CSF-1 receptor improves the antitumor efficacy of adoptive cell transfer immunotherapy. Cancer Res. 2014;74: 153–161. doi:10.1158/0008-5472.CAN-13-1816

21. Tagliani E, Shi C, Nancy P, Tay C-S, Pamer EG, Erlebacher A. Coordinate regulation of tissue macrophage and dendritic cell population dynamics by CSF-1. J Exp Med. 2011;208: 1901–1916. doi:10.1084/jem.20110866

22. Bruttger J, Karram K, Wörtge S, Regen T, Marini F, Hoppmann N, et al. Genetic Cell Ablation Reveals Clusters of Local Self-Renewing Microglia in the Mammalian Central Nervous System. Immunity. 2015;43: 92–106. doi:10.1016/j.immuni.2015.06.012

23. Biswas A, Bruder D, Wolf SA, Jeron A, Mack M, Heimesaat MM, et al. Ly6C high Monocytes Control Cerebral Toxoplasmosis. J Immunol. 2015;194: 3223–3235. doi:10.4049/jimmunol.1402037

24. Goldmann T, Wieghofer P, Müller PF, Wolf Y, Varol D, Yona S, et al. A new type of microglia gene targeting shows TAK1 to be pivotal in CNS autoimmune inflammation. Nat Neurosci. 2013;16: 1618–1626. doi:10.1038/nn.3531

25. Butovsky O, Jedrychowski MP, Moore CS, Cialic R, Lanser AJ, Gabriely G, et al.

686 Identification of a unique TGF-β-dependent molecular and functional signature in
687 microglia. Nat Neurosci. 2014;17: 131–43. doi:10.1038/nn.3599
688 26. Krasemann S, Madore C, Cialic R, Baufeld C, Calcagno N, El Fatimy R, et al. The
689 TREM2-APOE Pathway Drives the Transcriptional Phenotype of Dysfunctional Microglia
690 in Neurodegenerative Diseases. Immunity. 2017;47: 566-581.e9.
691 doi:10.1016/j.immuni.2017.08.008
692 27. Keren-shaul H, Spinrad A, Weiner A, Colonna M, Schwartz M, Amit I, et al. Article A
693 Unique Microglia Type Associated with Restricting Development of Alzheimer ' s Disease
694 Article A Unique Microglia Type Associated with Restricting Development of Alzheimer ' s
695 Disease. 2017; 1276–1290. doi:10.1016/j.cell.2017.05.018
696 28. Krasemann S, Madore C, Cialic R, Baufeld C, Calcagno N, El Fatimy R, et al. The
697 TREM2-APOE Pathway Drives the Transcriptional Phenotype of Dysfunctional Microglia
698 in Neurodegenerative Diseases. Immunity. 2017;47: 566-581.e9.
699 doi:10.1016/j.immuni.2017.08.008
700 29. Nathan CF, Murray HW, Wiebe ME, Rubin BY. Identification of interferon-gamma as the
701 lymphokine that activates human macrophage oxidative metabolism and antimicrobial
702 activity. J Exp Med. 1983;158: 670–689. doi:10.1084/jem.158.3.670
703 30. Murray HW, Spitalny GL, Nathan CF. Activation of mouse peritoneal macrophages in
704 vitro and in vivo by interferon-gamma. J Immunol. 1985;134: 1619 LP – 1622. Available:
705 http://www.jimmunol.org/content/134/3/1619.abstract
706 31. Pfefferkorn ER. Interferon gamma blocks the growth of Toxoplasma gondii in human
707 fibroblasts by inducing the host cells to degrade tryptophan. Proc Natl Acad Sci. 1984;81:
708 908–912. doi:10.1073/pnas.81.3.908
709 32. Strack A, Asensio V, Campbell I, Schlüter D, Deckert M. Chemokines are differentially
710 expressed by astrocytes, microglia and inflammatory leukocytes in Toxoplasma
711 encephalitis and critically regulated by interferon-γ. Acta Neuropathol. 2002;103: 458–

468. doi:10.1007/s00401-001-0491-7

33. Kamijo R, Harada H, Matsuyama T, Bosland M, Gerecitano J, Shapiro D, et al. Requirement for Transcription Factor IRF-1 in NO Synthase Induction in Macrophages. Science (80-). 1994;263: 1612–1615. doi:10.1126/science.7510419

34. Gao J, Morrison DC, Parmely TJ, Russell SW, Murphy WJ. An Interferon-γ-activated Site (GAS) Is Necessary for Full Expression of the Mouse iNOS Gene in Response to Interferon-γ and Lipopolysaccharide. J Biol Chem. 1997;272: 1226–1230. doi:10.1074/jbc.272.2.1226

35. Roche PA, Cresswell P. Antigen Processing and Presentation Mechanisms in Myeloid Cells. Myeloid Cells in Health and Disease. Washington, DC, USA: ASM Press; 2017. pp. 209–223. doi:10.1128/9781555819194.ch11

36. Lee YJ, Benveniste EN. Stat1 alpha expression is involved in IFN-gamma induction of the class II transactivator and class II MHC genes. J Immunol. 1996;157: 1559 LP – 1568. Available: http://www.jimmunol.org/content/157/4/1559.abstract

37. Christova R, Jones T, Wu P-J, Bolzer A, Costa-Pereira AP, Watling D, et al. P -STAT1 mediates higher-order chromatin remodelling of the human MHC in response to IFNγ. J Cell Sci. 2007;120: 3262–3270. doi:10.1242/jcs.012328

38. Muhlethaler-Mottet A, Di Berardino W, Otten LA, Mach B. Activation of the MHC Class II Transactivator CIITA by Interferon-γ Requires Cooperative Interaction between Stat1 and USF-1. Immunity. 1998;8: 157–166. doi:10.1016/S1074-7613(00)80468-9

39. Yona S, Kim KW, Wolf Y, Mildner A, Varol D, Breker M, et al. Fate Mapping Reveals Origins and Dynamics of Monocytes and Tissue Macrophages under Homeostasis. Immunity. 2013;38: 79–91. doi:10.1016/j.immuni.2012.12.001

40. Norris G, Derecki N, Kipnis J. Microglial Sholl Analysis. Protoc Exch. 2014. doi:10.1038/protex.2014.029

41. Fox BA, Gigley JP, Bzik DJ. Toxoplasma gondii lacks the enzymes required for de novo

arginine biosynthesis and arginine starvation triggers cyst formation. Int J Parasitol. 2004;34: 323–331. doi:10.1016/j.ijpara.2003.12.001

42. Colasanti M, Salvati L, Venturini G, Ascenzi P, Gradoni L. Cysteine protease as a target for nitric oxide in parasitic organisms. Trends Parasitol. 2001;17: 575. doi:10.1016/S1471-4922(01)02191-2

43. Xu W, Comhair SAA, Zheng S, Chu SC, Marks-Konczalik J, Moss J, et al. STAT-1 and c-Fos interaction in nitric oxide synthase-2 gene activation. Am J Physiol Cell Mol Physiol. 2003;285: L137–L148. doi:10.1152/ajplung.00441.2002

44. Chao, C. C., Anderson, R., Hu, S., Genker, G., Martella, A. and Peterson PK. Activated microglia inhibit multiplication of Toxoplasma gondii via a nitric oxide mechanism. Clinical Immunology and Immunopathology. Clin Immunol Immunopathol. 1993; 178–183.

45. Scharton-Kersten TM, Yap G, Magram J, Sher A. Inducible Nitric Oxide Is Essential for Host Control of Persistent but Not Acute Infection with the Intracellular Pathogen *Toxoplasma gondii*. J Exp Med. 1997;185: 1261–1274. doi:10.1084/jem.185.7.1261

46. Mundt S, Mrdjen D, Utz SG, Greter M, Schreiner B, Becher B. Conventional DCs sample and present myelin antigens in the healthy CNS and allow parenchymal T cell entry to initiate neuroinflammation. Sci Immunol. 2019. doi:10.1126/sciimmunol.aau8380

47. Suzuki Y, Sa Q, Gehman M, Ochiai E. Interferon-gamma- and perforin-mediated immune responses for resistance against Toxoplasma gondii in the brain. Expert Rev Mol Med. 2011;13: e31. doi:10.1017/S1462399411002018

48. Ochiai E, Sa Q, Brogli M, Kudo T, Wang X, Dubey JP, et al. CXCL9 is important for recruiting immune T cells into the brain and inducing an accumulation of the T cells to the areas of tachyzoite proliferation to prevent reactivation of chronic cerebral infection with Toxoplasma gondii. Am J Pathol. 2014;185: 314–324. doi:10.1016/j.ajpath.2014.10.003

49. Harris TH, Banigan EJ, Christian DA, Konradt C, Wojno EDT, Norose K, et al. Generalized Lévy walks and the role of chemokines in migration of effector CD8 + T cells.

764 Nature. 2012;486: 545–548. doi:10.1038/nature11098

765 50. Jebbari, H., Roberts, C.W., Ferguson D.J., Bluethmann, H., Alexander J. A protective role
766 for IL-6 during early infection with Toxoplasma gondii. Parasite Immunol. 1998;20: 231–
767 239. doi:10.1046/j.1365-3024.1998.00152.x

768 51. Chang HR, Grau GE, Pechère JC. Role of TNF and IL-1 in infections with Toxoplasma
769 gondii. Immunology. 1990;69: 33–7. Available:
770 http://www.ncbi.nlm.nih.gov/pubmed/2107144

771 52. Wang X, Michie SA, Xu B, Suzuki Y. Importance of IFN- γ -Mediated Expression of
772 Endothelial VCAM-1 on Recruitment of CD8 + T Cells into the Brain During Chronic
773 Infection with Toxoplasma gondii. J Interf Cytokine Res. 2007;27: 329–338.
774 doi:10.1089/jir.2006.0154

775 53. Taylor GA, Collazo CM, Yap GS, Nguyen K, Gregorio TA, Taylor LS, et al. Pathogen-
776 specific loss of host resistance in mice lacking the IFN-γ-inducible gene IGTP. Proc Natl
777 Acad Sci. 2000;97: 751–755. doi:10.1073/pnas.97.2.751

778 54. Zhao YO, Khaminets A, Hunn JP, Howard JC. Disruption of the Toxoplasma gondii
779 parasitophorous vacuole by IFNγ-inducible immunity-related GTPases (IRG proteins)
780 triggers necrotic cell death. PLoS Pathog. 2009;5. doi:10.1371/journal.ppat.1000288

781 55. Selleck EM, Fentress SJ, Beatty WL, Degrandi D, Pfeffer K, Virgin HW, et al. Guanylate-
782 binding Protein 1 (Gbp1) Contributes to Cell-autonomous Immunity against Toxoplasma
783 gondii. Yap GS, editor. PLoS Pathog. 2013;9: e1003320.
784 doi:10.1371/journal.ppat.1003320

785 56. Degrandi D, Kravets E, Konermann C, Beuter-Gunia C, Klumpers V, Lahme S, et al.
786 Murine Guanylate Binding Protein 2 (mGBP2) controls Toxoplasma gondii replication.
787 Proc Natl Acad Sci. 2013;110: 294–299. doi:10.1073/pnas.1205635110

788 57. Johnston AC, Piro A, Clough B, Siew M, Virreira Winter S, Coers J, et al. Human GBP1
789 does not localize to pathogen vacuoles but restricts Toxoplasma gondii. Cell Microbiol.

2016;18: 1056–1064. doi:10.1111/cmi.12579

58. Ferguson DJ, Graham DI, Hutchison WM. Pathological changes in the brains of mice infected with Toxoplasma gondii: a histological, immunocytochemical and ultrastructural study. Int J Exp Pathol. 1991;72: 463–74. Available: http://www.ncbi.nlm.nih.gov/pubmed/1883744

59. Soête M, Dubremetz JF. Toxoplasma gondii: Kinetics of Stage-Specific Protein Expression During Tachyzoite-Bradyzoite Conversion in Vitro. Toxoplasma gondii. Berlin, Heidelberg: Springer Berlin Heidelberg; 1996. pp. 75–80. doi:10.1007/978-3-642-51014-4_8

60. Mahittikorn A, Wickert H, Sukthana Y. Toxoplasma gondii: Simple duplex RT-PCR assay for detecting SAG1 and BAG1 genes during stage conversion in immunosuppressed mice. Exp Parasitol. 2010;124: 225–231. doi:10.1016/j.exppara.2009.10.003

61. Abdelbaset AE, Fox BA, Karram MH, Abd Ellah MR, Bzik DJ, Igarashi M. Lactate dehydrogenase in Toxoplasma gondii controls virulence, bradyzoite differentiation, and chronic infection. Hakimi MA, editor. PLoS One. 2017;12: e0173745. doi:10.1371/journal.pone.0173745

62. Yona S, Kim KW, Wolf Y, Mildner A, Varol D, Breker M, et al. Fate Mapping Reveals Origins and Dynamics of Monocytes and Tissue Macrophages under Homeostasis. Immunity. 2013;38: 79–91. doi:10.1016/j.immuni.2012.12.001

63. Goldmann T, Wieghofer P, Jordão MJC, Prutek F, Hagemeyer N, Frenzel K, et al. Origin, fate and dynamics of macrophages at central nervous system interfaces. Nat Immunol. 2016;17: 797–805. doi:10.1038/ni.3423

64. Hidano S, Randall LM, Dawson L, Dietrich HK, Konradt C, Klover PJ, et al. STAT1 signaling in astrocytes is essential for control of infection in the central nervous system. MBio. 2016;7: 1–15. doi:10.1128/mBio.01881-16

65. Davalos D, Grutzendler J, Yang G, Kim J V., Zuo Y, Jung S, et al. ATP mediates rapid

816 microglial response to local brain injury in vivo. Nat Neurosci. 2005;8: 752–758.
817 doi:10.1038/nn1472
818 66. Hickman SE, Kingery ND, Ohsumi TK, Borowsky ML, Wang L, Means TK, et al. The
819 microglial sensome revealed by direct RNA sequencing. Nat Neurosci. 2013;16: 1896.
820 Available: https://doi.org/10.1038/nn.3554
821 67. Roth TL, Nayak D, Atanasijevic T, Koretsky AP, Latour LL, McGavern DB. Transcranial
822 amelioration of inflammation and cell death after brain injury. Nature. 2014;505: 223–228.
823 doi:10.1038/nature12808
824 68. Lou N, Takano T, Pei Y, Xavier AL, Goldman SA, Nedergaard M. Purinergic receptor
825 P2RY12-dependent microglial closure of the injured blood–brain barrier. Proc Natl Acad
826 Sci. 2016;113: 1074–1079. doi:10.1073/pnas.1520398113
827 69. Lavin Y, Winter D, Blecher-Gonen R, David E, Keren-Shaul H, Merad M, et al. Tissue-
828 resident macrophage enhancer landscapes are shaped by the local microenvironment.
829 Cell. 2014;159: 1312–1326. doi:10.1016/j.cell.2014.11.018
830 70. van de Laar L, Saelens W, De Prijck S, Martens L, Scott CL, Van Isterdael G, et al. Yolk
831 Sac Macrophages, Fetal Liver, and Adult Monocytes Can Colonize an Empty Niche and
832 Develop into Functional Tissue-Resident Macrophages. Immunity. 2016;44: 755–768.
833 doi:10.1016/j.immuni.2016.02.017
834

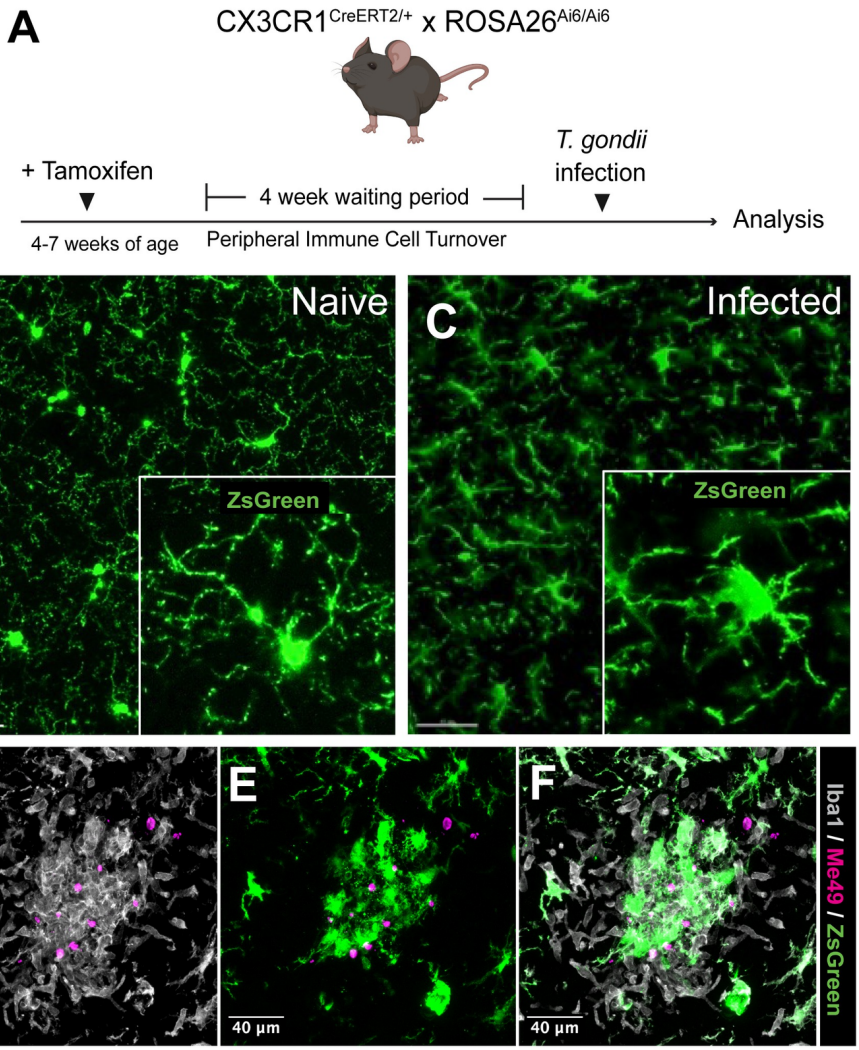

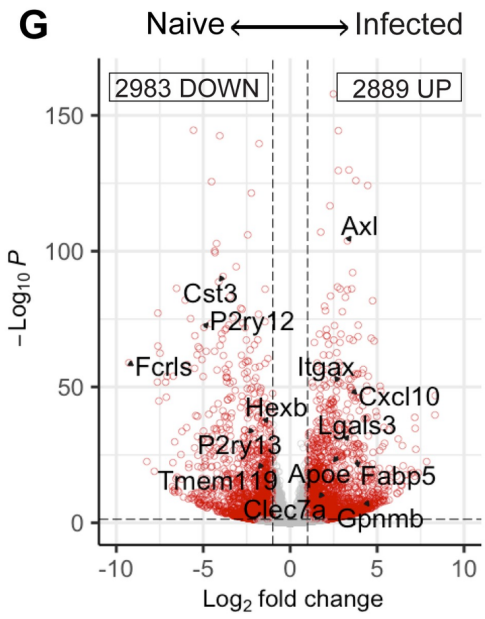

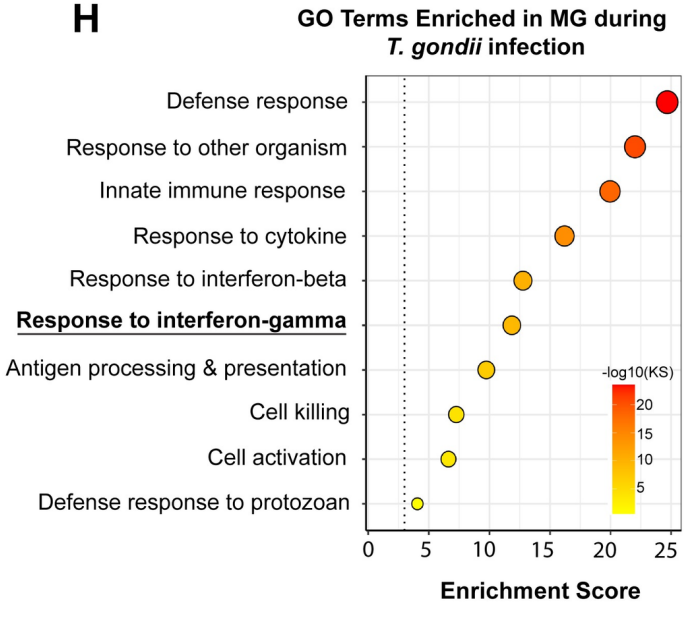

836 **Fig. 1 Microglial activation and recruitment *to T. gondii* foci within the brain.** WT microglia
837 reporter mice were infected with 10 cysts of the Me49 strain of *T. gondii* and were analyzed
838 against naïve controls using IHC and bulk RNA-sequencing. **(A)** Schematic outline for generating
839 microglia reporter mice. **(B, C)** Representative confocal micrographs with zoomed insets of
840 ZsGreen+ microglia (green) in naïve mice **(B)** and at 15 DPI **(C),** illustrating transition to amoeboid
841 morphology. **(D – F)** Representative confocal micrograph of microglial / macrophage clustering in
842 *T. gondii* foci**.** Brain sections were immuno-stained for Iba1 (gray) and Me49 (magenta). **(G)** Gene
843 ontology terms for biological processes statistically over-represented in microglia at 28 DPI,
844 relative to naïve state. GO terms were selected based on interest and plotted with enrichment
845 scores that indicate the $-\log_{10}$ of enrichment *p* value, based on Kolmogorov-Smirnov (KS)
846 analysis. Scale bars indicate 20 μm **(B – C)** or 40 μm (**D-F**).
847

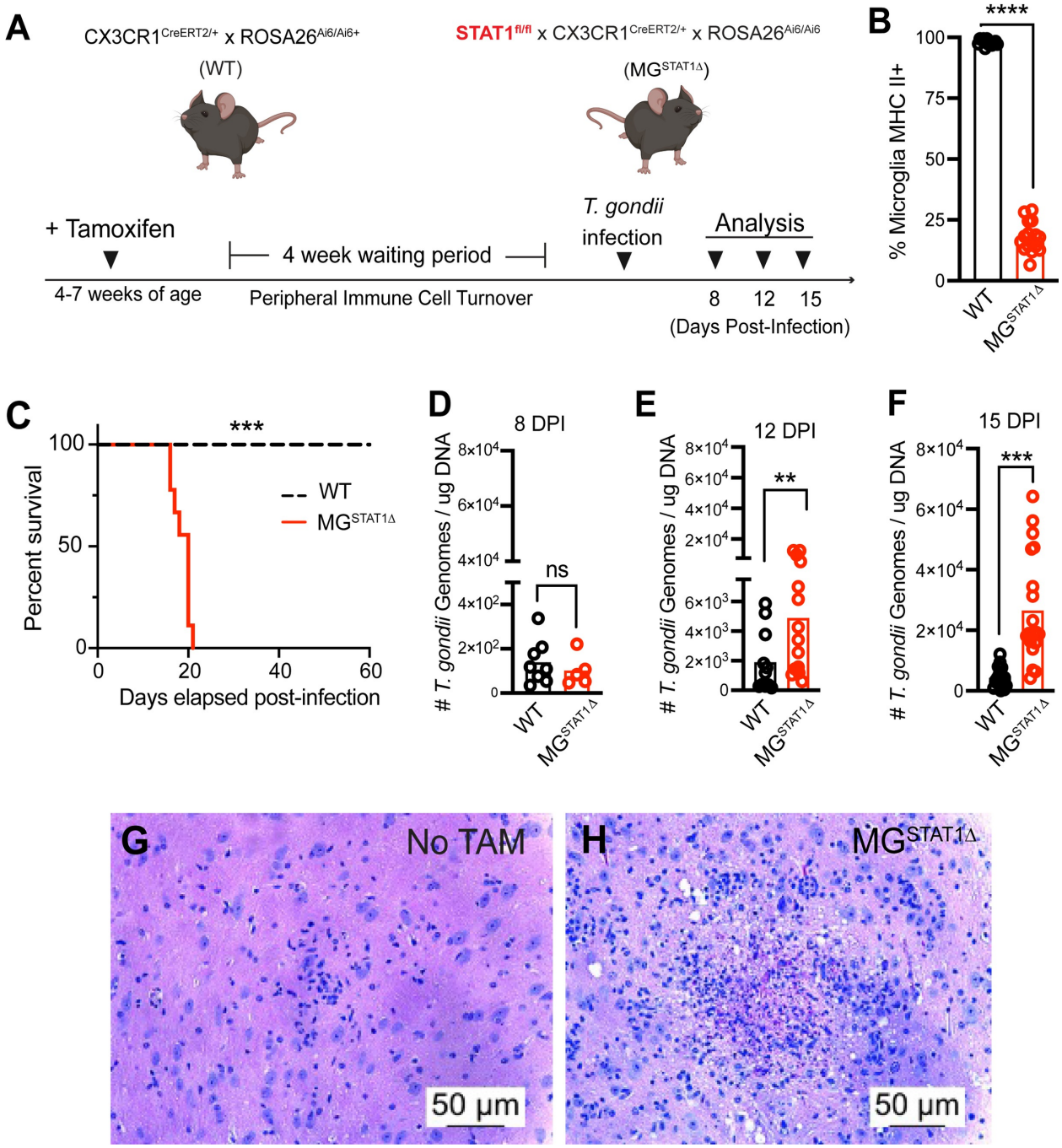

Fig. 2 Mice with STAT1-deficient microglia succumb to fatal toxoplasmic encephalitis. (A-F) Tamoxifen-treated CX3CR1$^{CreERT2/+}$ x ROSA26$^{Ai6/Ai6}$ (WT) and STAT1$^{fl/fl}$ x CX3CR1$^{CreERT2/+}$ x ROSA26$^{Ai6/Ai6}$ (MG^{STAT1Δ}) mice were intraperitoneally infected with 10 cysts of the Me49 strain of *T. gondii* and analyzed at 8, 12, and 15 DPI. **(A)** Schematic for generating WT and MG^{STAT1Δ} mice. **(B)** Flow cytometric quantification of microglial MHC II expression, as a functional readout for

854 STAT1 excision. **(C)** Animal survival curve of WT and MG$^{STAT1\Delta}$ following *T. gondii* challenge. **(D**
855 **– F)** qPCR analysis of *T. gondii* brain parasite burden quantified by qPCR analysis of
856 homogenized brain tissue at 8- **(D)**, 12- **(E)**, and 15- **(F)** DPI. (**G, H**) Representative brain
857 histopathology observed via H&E staining in litter-mate vehicle **(G)** or tamoxifen-treated MG$^{STAT1\Delta}$
858 mice at 15 DPI. ns = not significant, ** = $p < 0.01$, *** = $p < 0.001$, **** = $p < 10^{-4}$. Statistical
859 significance was determined by two-way randomized block ANOVA **(B, D-F)** or Kaplan-Meier
860 analysis with total n = 26 from 4 pooled experiments **(B)**, *n* = 13 from 2 experiments (**C**) *n* = 15
861 from 2 experiments, **(E)**, *n* = 26 from 3 experiments **(F)**, and *n* = 38 from 4 experiments. Scale bar
862 = 50 um.
863
864

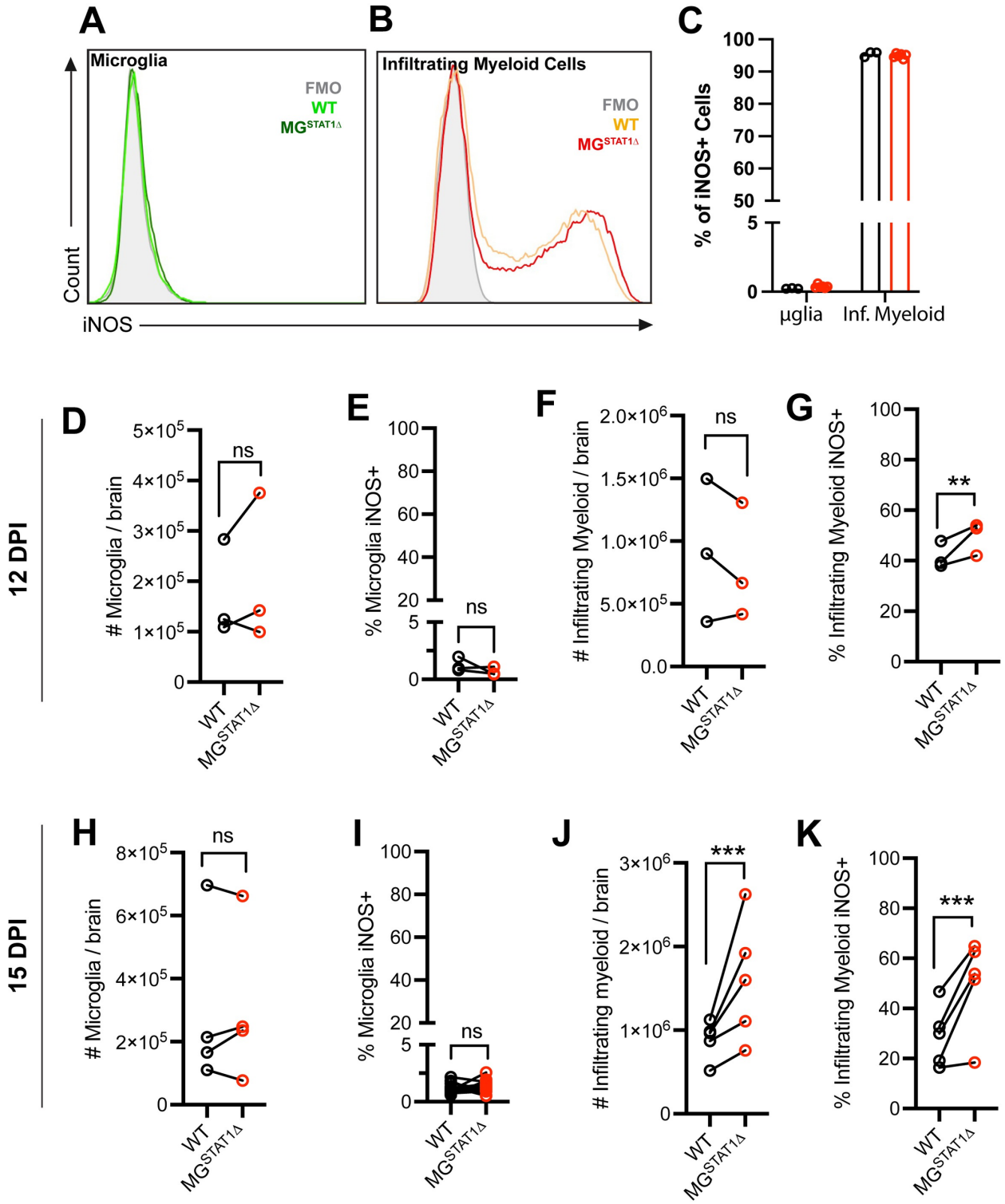

Fig. 3 Brain-infiltrating myeloid cells, but not brain-resident microglia, express iNOS during *T. gondii* challenge. WT and MG$^{STAT1\Delta}$ mice were intraperitoneally infected with 10 cysts of the Me49 strain of *T. gondii* and brains were analyzed by flow cytometry. Representative histograms

indicating iNOS expression in ZsGreen+ CD11b+ CD45int brain-resident microglia **(A)** and CD11b+ CD45hi Ly6C+ infiltrating myeloid cells **(B)** at 12 DPI. **(C)** Flow cytometric quantification of the total brain iNOS+ cells by myeloid population at 12 DPI. 12 DPI analysis of total number of microglia isolated per brain **(D)**, microglial iNOS frequency **(E)**, number of infiltrating myeloid cells isolated per brain **(F),** and infiltrating myeloid iNOS frequency **(G).** 15 DPI quantification of total number of microglia isolated per brain **(H)**, microglial iNOS frequency **(I)**, number of infiltrating myeloid cells isolated per brain **(J),** and infiltrating myeloid iNOS frequency **(K)**. ns = not significant, ** = $p < 0.01$, *** = $p < 0.001$, **** = $p < 10^{-4}$. Statistical significance was determined by two-way randomized block ANOVA (**D-K**). n = 3-5 per group (**C**), and total n = 19 (**D-F**), total n = 22 (**E-G**), n = 31 (**H-I**), and n = 38 (**J-K**). **(B-K)** Biological replicates are individual mice, with group means from individual experiments plotted as open circles with black lines connecting experimental and control groups. Data are pooled from 3 experiments (**D-G**), 4 experiments (**H-I**), or 5 experiments (**J-K**). Source data (**D-K**) are provided in a source data file.

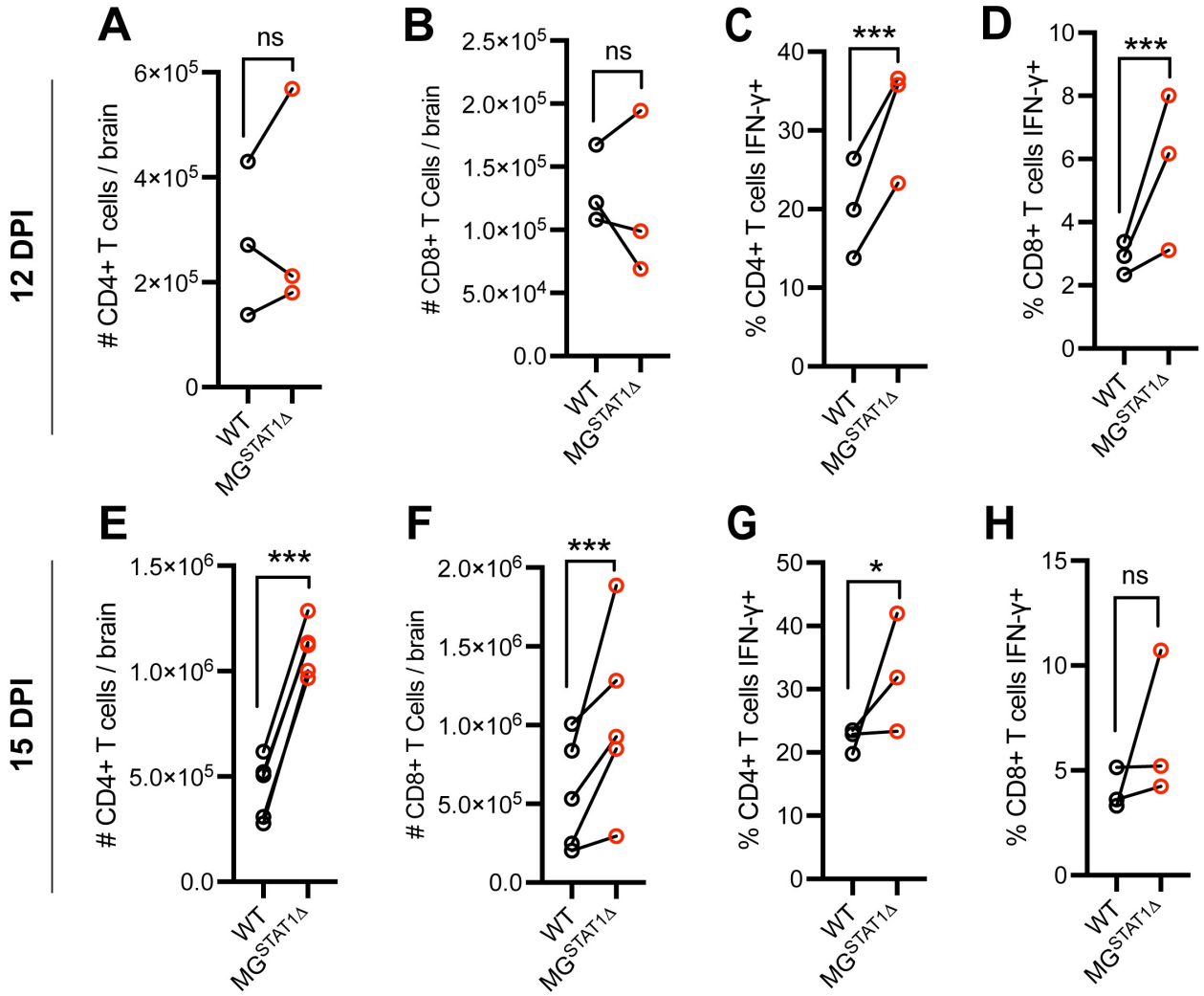

Fig. 4 Brain T cell responses are potentiated in MG$^{STAT1\Delta}$ mice relative to WT controls. WT and MG$^{STAT1\Delta}$ mice were intraperitoneally infected with 10 cysts of the Me49 strain of *T. gondii* and brains were analyzed by flow cytometry at 12 and 15 DPI. (**A-B**) CD3+CD4+ and CD3+CD8+ cell count enumerated for whole brain and (**C–D**) IFN-γ protein expression at 12 DPI. (**E-F**) CD3+CD4+ and CD3+CD8+ cell count enumerated for whole brain and (**G-H**) IFN-γ protein expression at 15 DPI. ns = not significant, and *** = $p < 0.001$. Statistical significance was determined by two-way randomized block ANOVA. Data are pooled from 3 (**A-D** & **G-H**), or 4 (**E-F**) separate experiments, with total *n* = 19 (**A-B**), *n* = 24 (**C-D**), *n* = 28 (**E-F**), and *n* = 21 (**G-H**). Biological replicates are individual mice, with group means from individual experiments plotted as

894 open circles with black lines connecting experimental and control groups. Source data (**A-H**) are

895 provided in a source data file.

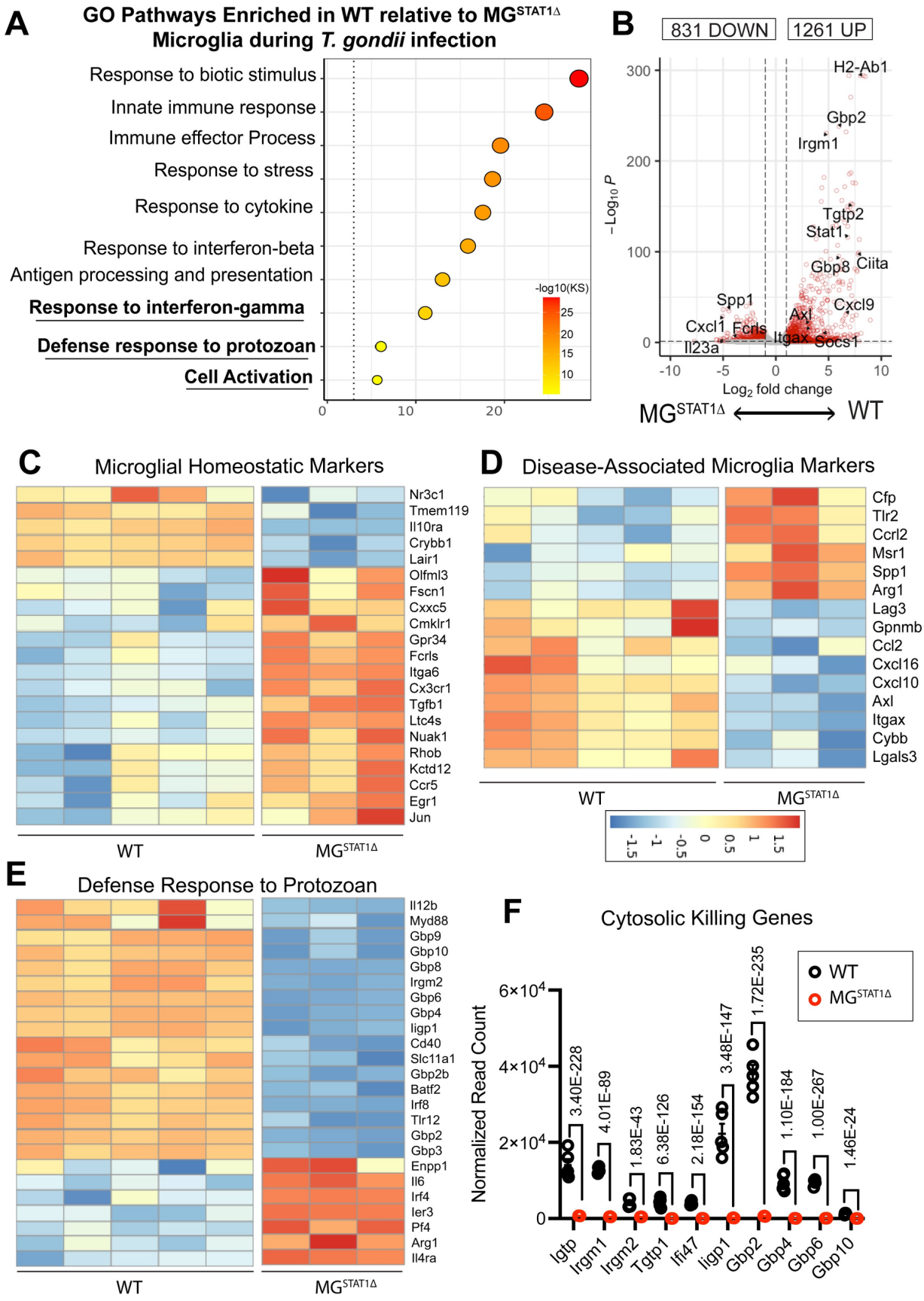

Fig. 5 STAT1-deficient microglia fail to upregulate genes encoding critical anti-parasitic cytosolic proteins. WT and $MG^{STAT1\Delta}$ mice were intraperitoneally infected with 10 cysts of the Me49 strain of *T. gondii*, and brain-resident microglia were FACS-sorted and RNA-sequenced at 12 DPI. (**A**) Gene ontology (GO) terms statistically enriched in WT relative to $MG^{STAT1\Delta}$ microglia. GO terms were selected based on interest and plotted enrichment scores indicate the $-\log_{10}$ of enrichment p value, based on Kolmogorov-Smirnov (KS) analysis. (**B**) Volcano plot. (**C-D)** Heat maps displaying VST-normalized, hierarchically-clustered significantly differentially expressed microglial homeostatic genes (**C**) and disease-associated microglia genes (**D**) previously reported as markers of disease-associated microglia (DAM) across neuroinflammatory conditions. (**E**) Heatmap displaying genes from the GO Term “Defense response to protozoan” (GO:0042832) in WT vs. $MG^{STAT1\Delta}$ mice. (**F**) Normalized read count of IRG- and GBP-family proteins expressed by microglia and differentially regulated by STAT1, with *p* values indicating BH-adjusted *p*-values from the full gene expression analysis in DESeq2.

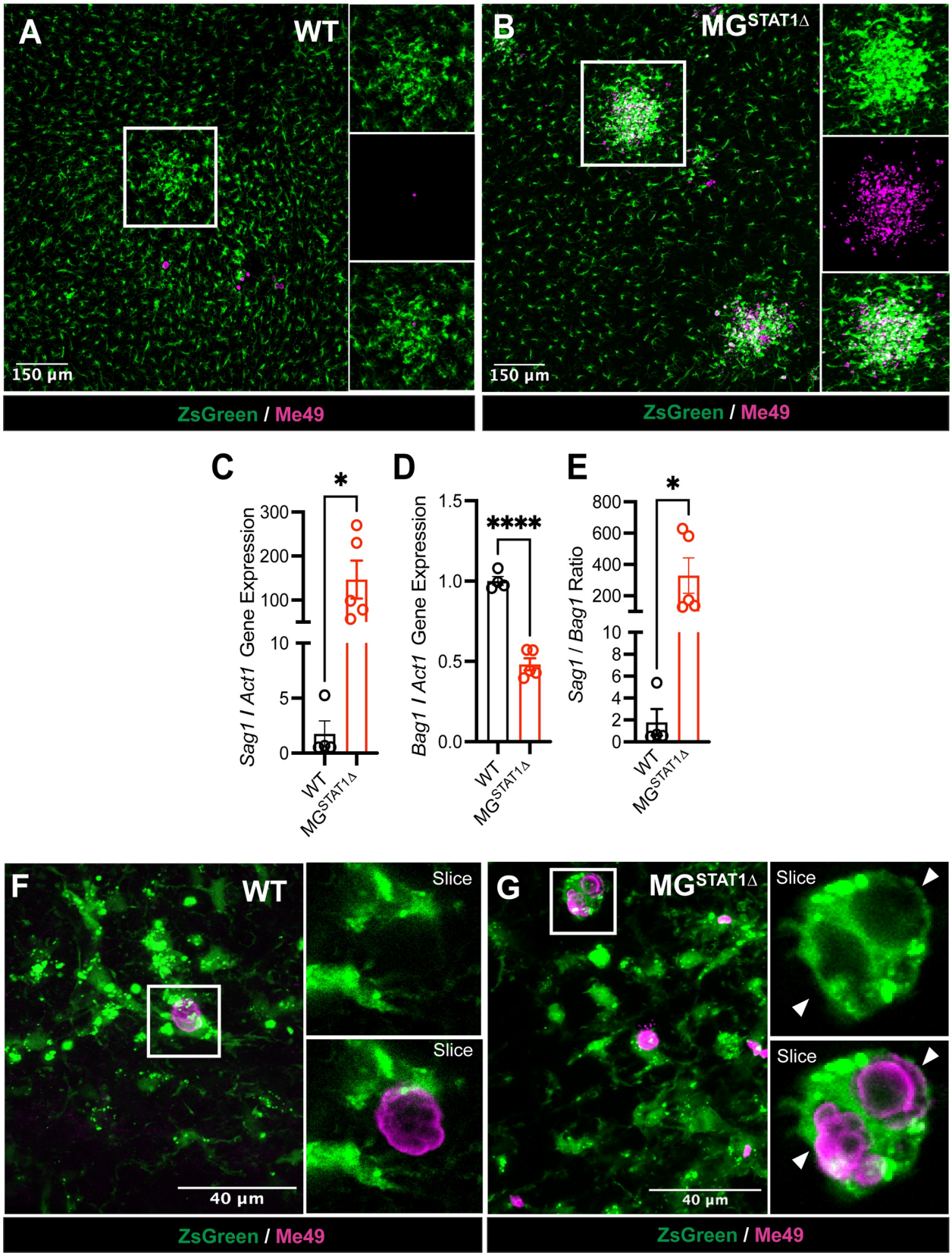

913 **Fig. 6 Microglial STAT1-deficiency results in a skewing of *T. gondii* toward its replicative**
914 **form.** WT and MG$^{STAT1\Delta}$ mice were intraperitoneally infected with 10 cysts of the Me49 strain of
915 *T. gondii* and brains were analyzed by confocal microscopy and RT-qPCR at 15 DPI. (**A-B**)
916 Representative 10x immunofluorescent confocal Z-stack images of *T. gondii* inflammatory foci in
917 infected brains. White square indicates example foci, with insets providing zoomed detail. (**C-E**)
918 RT-qPCR analysis of *T. gondii* relative gene expression of *Sag1* (tachyzoite-specific gene), *Bag1*
919 (bradyzoite-specific gene), and *Act1* (non-stage-specific gene) analyzed using *t* tests. (**F-G**)
920 Representative 40x Immunofluorescent images of microglial-parasite interactions in infected
921 brains. White square indicates *T. gondii* vacuole(s) in maximum projection view, with insets
922 providing zoomed detail in single-plane view (Slice). (**A-B**) and (**F-G**) ZsGreen is indicated green,
923 and anti-Me49 staining is indicated in magenta. Scale bar = 150 μm (**A-B**) and 40 μm (**F-G**). *n* =
924 3-4 mice per group (**C-E**). ns = not significant, * = $p < 0.05$, *** = $p < 0.001$.
925

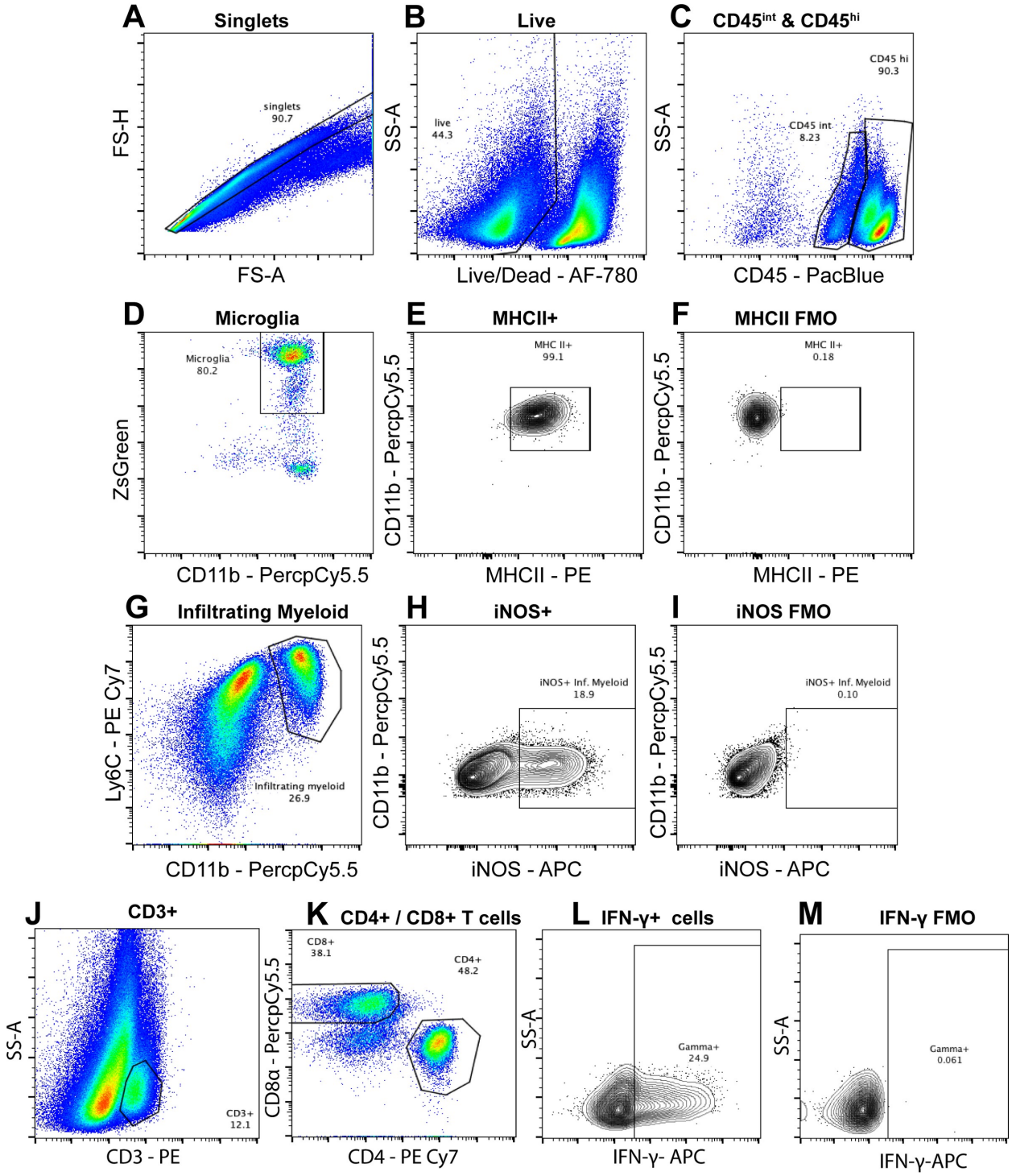

926

927 **Supplementary Figure 1 | Example gating strategy for brain immune cells**. Myeloid and T

928 cells isolated from mice with ZsGreen+ microglia were analyzed via flow cytometry. (**A-C**) For all

929 panels, cells were pre-gated on singlets (**A**), then live cells using a viability dye (**B**). (**C**) Cells were

930 gated to identify CD45 hi (brain-infiltrating) and CD45 int (brain-resident) immune cells. (**D**)

931 Microglia were gated based on CD45 intermediate expression, ZsGreen and CD11b expression,
932 and (**E-F**) MHC II positivity was assessed using FMO. (**G**) Infiltrating myeloid cells were gated
933 based on CD45 hi expression, and the expression of both CD11b and Ly6C. (**H-I**) iNOS
934 expression was determined via FMO gating. (**J-K**) T cells were gated based on the expression of
935 CD3 and CD4 or CD8. (**L-M**) IFN-γ expression on CD3+CD4+ and CD3+CD8+ cells was
936 determined based on FMO positivity.
937
938

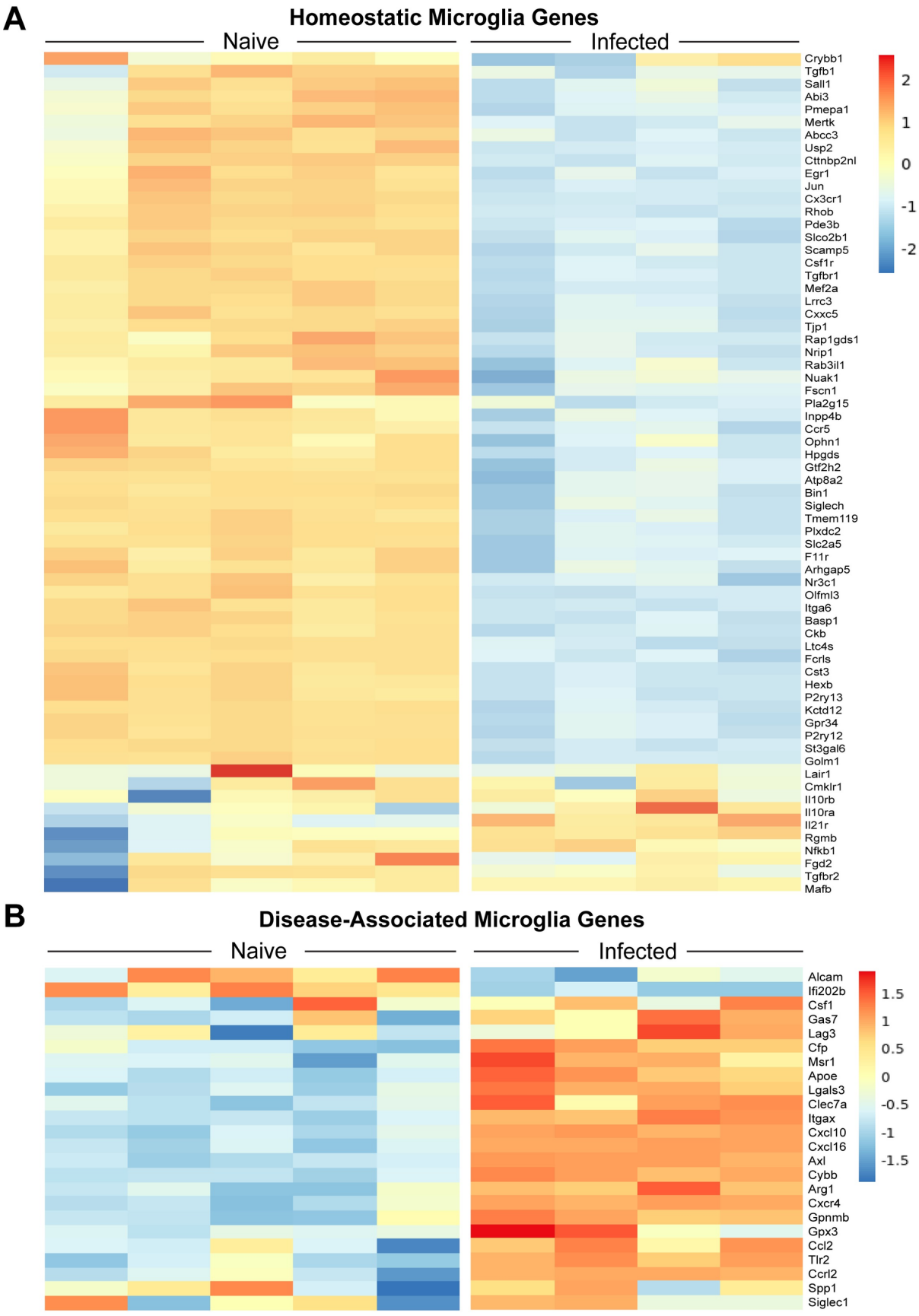

939

940

941 **Supplemental Figure 2 | RNA sequencing analysis of naïve vs. *T. gondii*-infected WT**
942 **microglia.** Microglia from wild-type naïve or wild-type mice infected with *T. gondii* for 4 weeks
943 were FACS-sorted and RNA-sequenced at 4 weeks post-infection. (**A-B)** Heat maps displaying
944 hierarchically-clustered gene expression from regularized log transformed gene abundance
945 counts. Heatmap data display the full set of significantly differentially expressed microglial
946 homeostatic genes (**A**), or disease-associated microglia genes (**B**), shared across
947 neurodegenerative models investigated in *Krasemann et al., 2017* and reflected in the naïve vs.
948 T*. gondii*-infected DESeq2 dataset. Statistical significance was defined in the differential gene
949 expression analysis as a BH adjusted p value < 0.05. n = 4-5 mice per group.

950

951

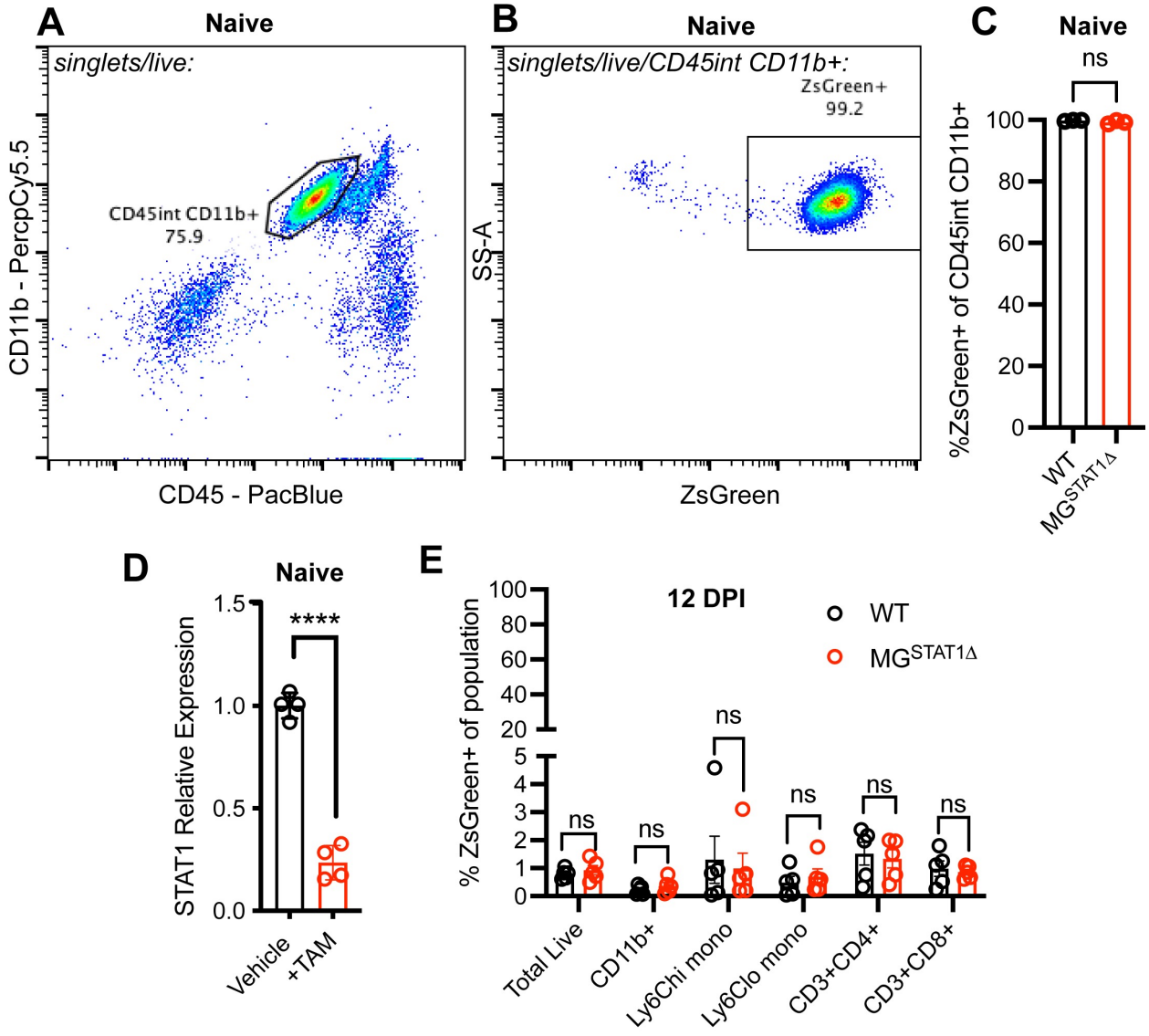

Supplemental Figure 3 | Validation of cre activity and STAT1 excision in MG$^{STAT1\Delta}$ mice. Naïve microglia and microglia isolated from brains at 12 DPI were analyzed by flow cytometry or RT-qPCR for relative gene expression. (**A-B**) Representative FACS plots indicating gating strategy for validating microglial ZsGreen expression in naïve mice. (**C**) Flow cytometric quantification of ZsGreen expression in total CD45^{int} CD11b+ cells in naïve WT or MG$^{STAT1\Delta}$ mice. (**D**) RT-qPCR quantification of *Stat1* relative expression in microglia that were magnetically enriched from naïve vehicle or tamoxifen (TAM)-treated MG$^{STAT1\Delta}$ mice. (**E**) Flow cytometric quantification of ZsGreen expression in various immune populations isolated from blood at 12

961 DPI, in WT or MG$^{STAT1\Delta}$ mice. Statistical significance was determined via unpaired *t* test (**C-E**),

962 with *n* = 3-5 mice per group (**C-E**). ns = not significant; **** = $p < 10^{-4}$.

963

964

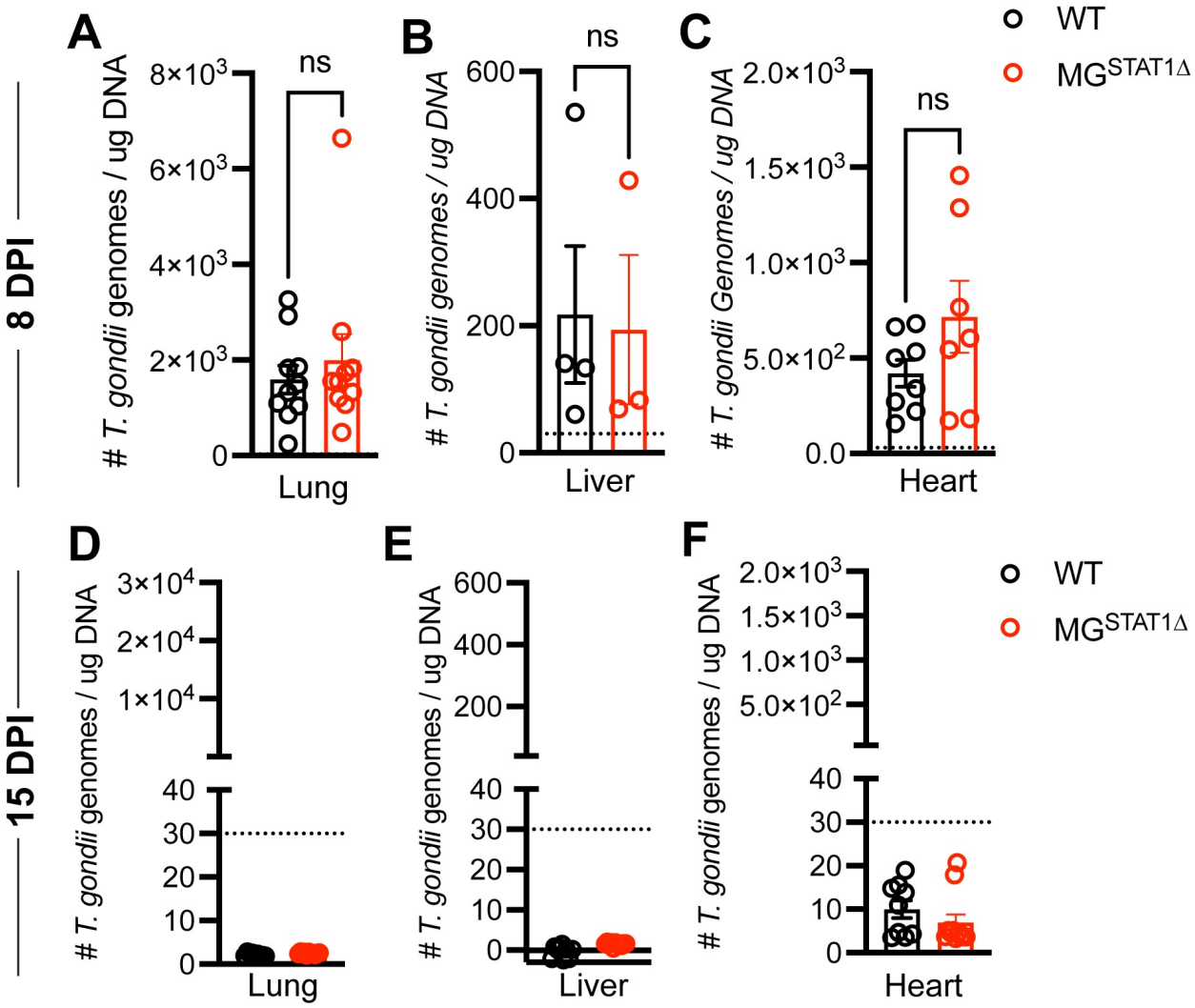

965

966 **Supplemental Figure 4 | *T. gondii* burden in peripheral tissues in WT and MG$^{STAT1\Delta}$ mice.**
967 WT and MG$^{STAT1\Delta}$ mice were intraperitoneally infected with 10 cysts of the Me49 strain of *T. gondii,*
968 and peripheral tissues were harvested and analyzed by qPCR for parasite genomic DNA, relative
969 to total tissue DNA. Parasite burden was quantified at 8 DPI in lung (**A**), liver (**B**), and heart (**C**)
970 tissue. Parasite burden was quantified at 15 DPI in lung (**D**), liver (**E**), and heart (**F**) tissue. (**A-C**)
971 Statistical significance was determined using randomized block ANOVA using compiled data from
972 2-3 experiments with total *n* = 20 (**A**) and total *n* = 15 (**C**), or via unpaired t test with *n* = 3-4 mice
973 per group (**B**). Dotted line on y axis denotes assay limit of detection, based on standard curve. ns
974 = not significant.

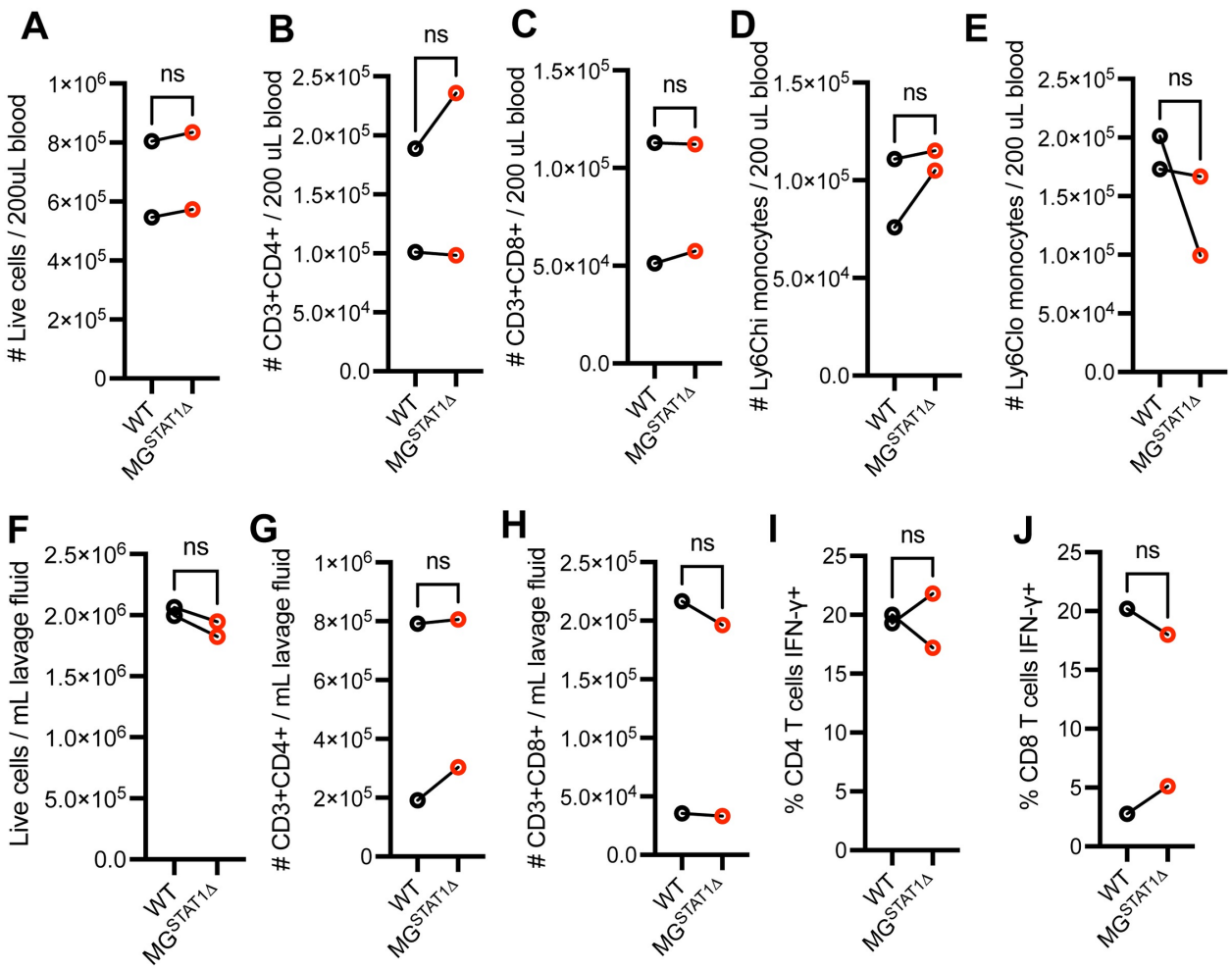

Supplemental Figure 5 | WT and MG$^{STAT1\Delta}$ mice display equivalent immune activation in peripheral tissues during *T. gondii* challenge. WT and MG$^{STAT1\Delta}$ mice were intraperitoneally infected with 10 cysts of the Me49 strain of *T. gondii,* and immune cells from blood and peritoneal fluid were analyzed by flow cytometry. (**A-E**) Flow cytometric quantification of total live immune cells (**A**), CD3+CD4+ T cell count (**B**), CD3+CD8+ T cell count (**C**), CD11b+Ly6Chi monocytes (**D**), and CD11b+Ly6Clo monocytes (**E**), calculated from blood. (**F-J**) Quantification of total live cells (**F**), number of CD3+CD4+ T cells, (**G**) number of CD3+CD8+ T cells (**H**), and CD4+ or CD8+ T cell expression of IFN-γ (**I-J**) isolated from the peritoneal cavity at 8 DPI. Statistical significance was determined by two-way randomized block ANOVA (**A-J**). ns = not significant, total *n* = 22

986 from two pooled experiments (**A-E**), or total *n* = 16 from two pooled experiments (**F-J**). Biological
987 replicates are individual mice, with group means from individual experiments plotted as open
988 circles with black lines connecting experimental and control groups. Source data (**A-H**) are
989 provided in a source data file.
990

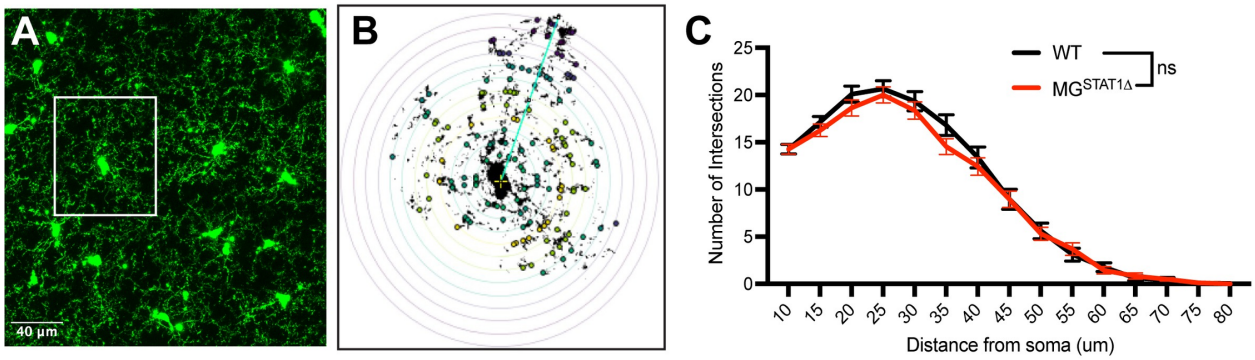

Supplementary Figure 6 | Morphometric analysis of WT and STAT1-deficient microglia. To analyze microglial activation, Sholl analysis was performed on microglia from the somatomotor cortex of naïve WT and $MG^{STAT1\Delta}$ mice. (**A**) ZsGreen+ microglia were imaged using a confocal microscope, and images were processed into a maximum projection using Fiji. (**B**) Images were made binary, microglia were manually isolated to determine cell process continuity, and the Sholl analysis Fiji plugin was executed to record intersections at varying soma distances. (**C**) Quantification of Sholl data via two-way ANOVA with Sidak's multiple comparisons test, *n* = 64-67 microglia from 3 mice per group. (**A**) Scale bar = 40 µm.

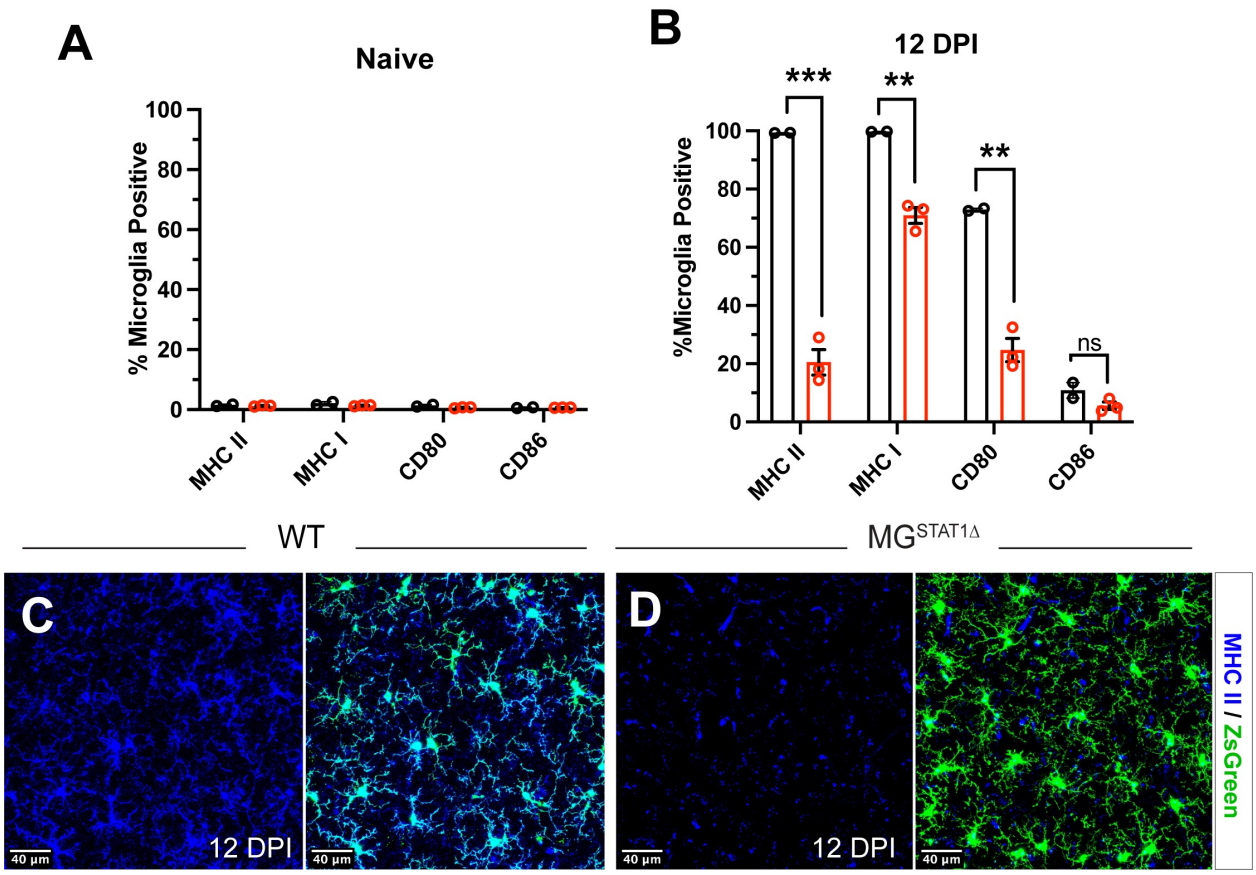

Supplemental Figure 7 | Microglial antigen presentation machinery is regulated by STAT1 during *T. gondii* infection. Microglia were isolated from naïve or 12 DPI infected WT or MG$^{STAT1\Delta}$ mouse brains and analyzed by flow cytometry and confocal microscopy. Flow cytometric analysis of microglial major histocompatibility complex and co-stimulatory molecules in (**A**) naïve brains, and (**B**) 12 DPI brains. (**C-D**) Immunohistochemical analysis of MHC II positivity by confocal microscopy; scale bar = 40 um, blue indicates MHC II, and green indicates ZsGreen fluorescence. *n* = 2-3 per group (**A-B**). ns = not significant, ** = p <0.01, *** = p < 0.001.

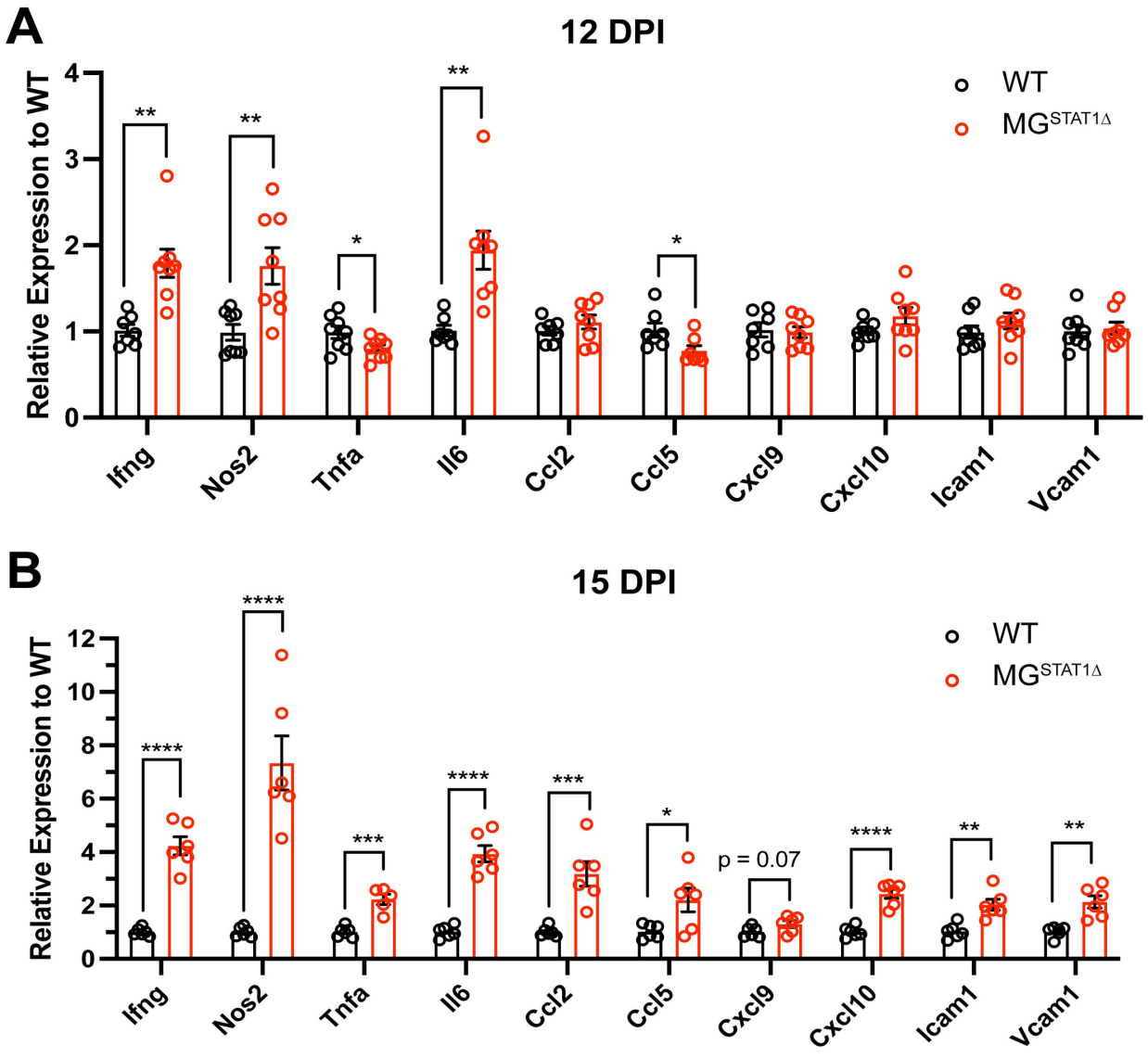

Supplemental Figure 8 | Whole brain RNA analysis of anti-parasitic defense genes. Whole brain homogenate from WT and MG$^{STAT1\Delta}$ mice was analyzed by RT-qPCR for a panel of various anti-parasitic genes. (**A**) 12 DPI and (**B**) 15 DPI immune effector profile. Statistical significance was determined by unpaired *t* test for one experiment (**A**), and two-way randomized block ANOVA from two pooled experiments (**B**). *n* = 8 per group (**A**), and total *n* = 19 (**B**). * = $p < 0.05$, ** = $p < 0.01$, *** = $p < 0.001$, **** = $p < 10^{-4}$. Error bars indicate standard error of the mean.

1024
1025
1026 **Supplementary Table 1**
1027

Reagent	Sequence
Toxo 529bp RE Forward Primer	5'-CAG TCC TGA TAT CTC TCC TCC AAG A-3'
Toxo 529bp RE Reverse Primer	5'- CAC AGA AGG GAC AGA AGT CGA A-3'
Toxo 529bp RE Probe	5'-/56-FAM/CTA CAG +A+CG+A+TGC C/3IABkFQ/-3'
Toxo Sag1 Forward Primer	5'-GGA TCG CCT GAG AAG CAT-3'
Toxo Sag1 Primer Reverse Primer	5'-ATG GAA ACG TGA CTG GCT-3'
Toxo Sag1 Probe	5'-/56-FAM/CT GTA CCG T/Zen/G CAA CTG GAG TTT GC/3IABkFQ/-3'
Toxo Bag1 Forward Primer	5'-CGT GGA GTT CGA CAG CAA-3'
Toxo Bag1 Reverse Primer	5'-ATA ACG ATG GCT CCG TTG TC-3'
Toxo Bag1 Probe	5'-/56-FAM/TT TGG CTG A/Zen/C TTG CCA GGT CTT CA/3IABkFQ/-3'
Toxo Act1 Forward Primer	5'-CGT GAG AGA ATG ACC CAG ATT AT-3'
Toxo Act1 Reverse Primer	5'-ACC GGA GGA GTA CAG AGA AA-3'
Toxo Act1 Probe	5'-/56-FAM/TC GAA ACC T/Zen/T TAA CGT CCC TGC CA/3IABkFQ/-3'

1028